ACS Catalysis

pubs.acs.org/acscatalysis

Research Article

Heterogeneous Pd-Catalyzed Efficient Synthesis of Imidazolones via Dehydrogenative Condensation between Ureas and 1,2-Diols

Juan Camilo Arango-Daza, Carles Lluna-Galán, Luis Izquierdo-Aranda, Jose R. Cabrero-Antonino,* and Rosa Adam*

Cite This: *ACS Catal.* 2022, 12, 6906−6922

Read Online

ACCESS | Metrics & More | Article Recommendations | Supporting Information

ABSTRACT: A heterogeneously catalyzed protocol for the acceptorless dehydrogenative condensation between *N*,*N*′-disubstituted ureas and 1,2-diols to afford imidazolones was developed. Palladium nanoaggregates stabilized onto an alumina matrix with suitable acidic properties, namely, [Pd/Al_2O_3], was designed and successfully applied as efficient and reusable heterogeneous nanocatalyst for this relevant transformation. The methodology developed showed its wide applicability through the synthesis of more than 25 imidazolones with moderate to good yields, reaching a turnover number (TON) of up to 19444 and a initial turnover frequency (TOF_0) > 290 h^{-1}. The active nanostructured catalyst was fully characterized [X-ray diffraction (XRD), high-resolution transmission electron microscopy (HR-TEM), high-resolution scanning transmission electron microscopy (HR-STEM), energy-dispersive X-ray (EDX), Raman spectroscopy, temperature-programmed reduction (TPR), temperature-programmed desorption (TPD)-NH_3, TPD-CO_2, X-ray photoelectron spectroscopy (XPS), Brunauer−Emmett−Teller (BET) area], and mechanistic studies were performed. Moreover, other related Pd-based nanomaterials composed of different acidic or basic inorganic supports were synthesized and extensively compared in this reaction. These studies revealed that the presence of Pd nanoparticles with a wide range of sizes (average particle size 2.8 nm) over a metal oxide support with a high density of acid sites is a key point for the good activity of the material, γ-Al_2O_3 being the optimum support. Furthermore, a Pd−Zn cooperation effect was described for the dehydrogenative condensation of unactivated 1,2-diols, including ethylene glycol, with ureas. Two Pd−Zn bimetallic materials ([Pd/ZnO] and [Pd(5%)−Zn(5%)/Al_2O_3]) were also designed and characterized properly. These materials, as well as the [Pd/Al_2O_3] system in combination with catalytic amounts of ZnO, showed good activity and selectivity in the acceptorless dehydrogenative condensation between ureas and unactivated 1,2-diols. The heterogeneous nature of all of the described catalytic systems was demonstrated, and the reusability of the catalysts was proven.

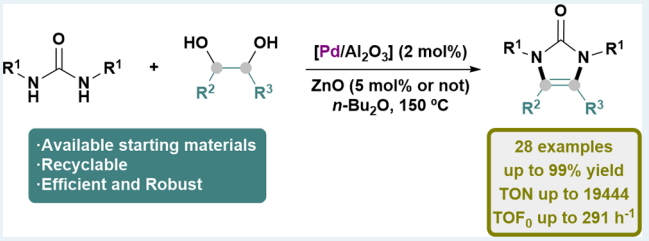

KEYWORDS: *heterogeneous catalysis, dehydrogenation, N-heterocycles, organic synthesis, palladium*

INTRODUCTION

The development of new methodologies to synthesize heterocycles that fulfill the requirements of green chemistry is a major goal in current organic chemistry and catalysis.[1] In this direction, acceptorless dehydrogenative reactions (AD) are especially interesting processes as they are atom-economical, do not need stoichiometric reagents or O_2, and generate only H_2 and H_2O as secondary products.[1a,c,m,2] Typically, in these transformations, an alcohol dehydrogenates affording H_2 and a carbonyl compound, which reacts with a coupling partner, generally an amine or another alcohol, to afford the desired condensation product. When applied intramolecularly or with ad hoc substrates, this method can easily afford heterocycles.[1a,c,m] A large variety of heterocycles have been obtained employing AD strategies with homogeneous catalysts. Pioneer examples in this area involved mainly Ru[3] and Ir[3e,4] complexes as catalysts. In the past years, important efforts have been made to substitute these precious metals for non-noble metals such as Co[5] or Mn.[6] However, these processes present obvious drawbacks from the sustainability viewpoint as they use metal complexes as catalysts, difficult to reuse, and frequently need basic additives. Hence, the development of solid nanostructured materials able to act as dehydrogenating catalysts in AD reactions affording heterocycles is of high interest.[1m,2d,7] Furthermore, the accurate design of these materials bearing multifunctional features in their structure and avoiding the use of external additives can entail a significant improvement of these processes.

Five-membered cyclic ureas, including imidazolones and imidazolidinones, are relevant heterocycles present in the structure of currently commercialized drugs such as

Received: March 23, 2022
Revised: May 7, 2022
Published: May 26, 2022

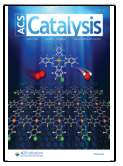

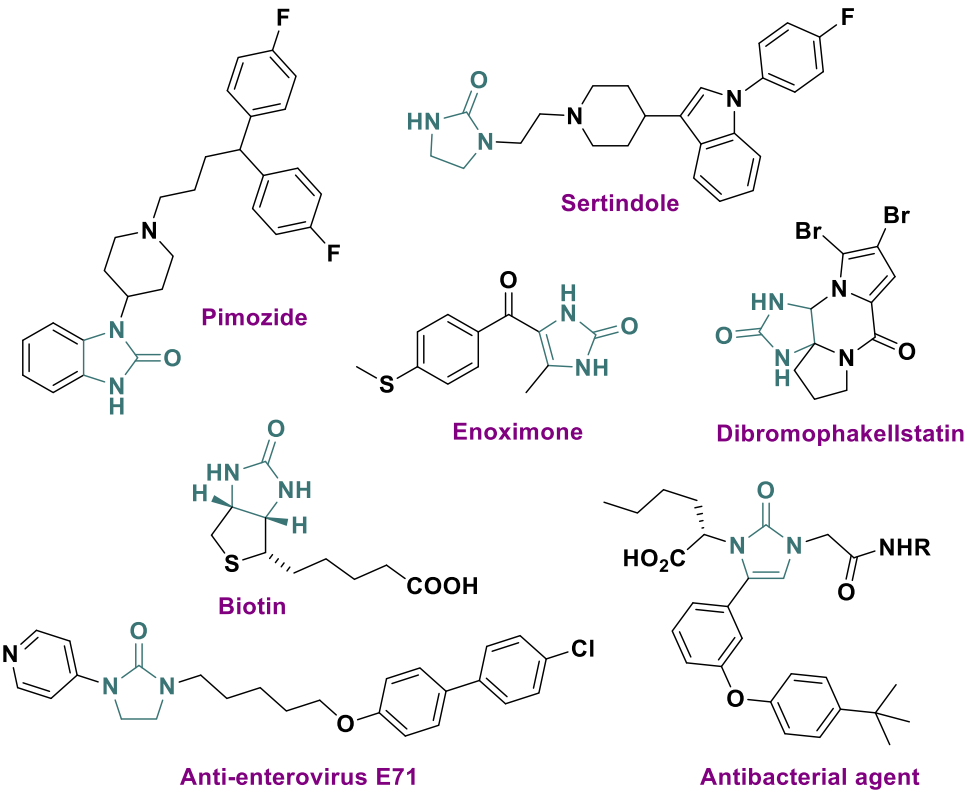

Figure 1. Imidazol(idin)one derivatives used as drugs or described as biologically active compounds.

enoximone,[8] a cardiovascular agent, or pimozide[9] and sertindole,[10] two antipsychotics (Figure 1). The imidazol(idin)one scaffold is also present in compounds with antiviral[11] or antibacterial[12] activities (Figure 1).

In addition, the cyclic urea structure can also be found in natural products such as dibromophakellstatin,[13] a molecule with antitumor activity, and biotin[14] or vitamin B7, key for the human metabolism (Figure 1). Hence, in the last two decades, several catalytic protocols have been investigated for the synthesis of imidazolones. Among these methodologies, hydroamidation of propargylic ureas,[15] diamination of olefins or aryl ketones with diaziridinones,[16] and diamine carbonylation[17] have been extensively developed. Despite their good applicability on a laboratory scale, these methods employ sophisticated molecules as starting materials or homogeneous species as catalysts. Other less developed methodologies involve heterocycles such as cyclic carbonates,[18] triazoles,[19] or hydantoins as starting materials.[20]

In this context, developing catalytic methodologies able to afford imidazolones from simple and readily accessible ureas and 1,2-diols via AD condensation is of high interest. Efforts in this area have been made by the group of Watanabe, who described in the 1990s the formation of imidazolones from ureas and 1,2-diols employing a homogeneous Ru complex as the catalyst (Scheme 1A).[3d] Very related to this, in 2016, Beller and co-workers published the formation of oxazolidinones from ureas and diols through a hydrogen-borrowing process.[21] In this work, the authors used a Ru complex as the catalyst, and an asymmetric version of the reaction was developed (Scheme 1B). In the heterogeneous catalysis area, only a few examples have been reported for the dehydrogenative activation of diols to afford heterocycles such as (aza)indoles,[7c,g,22] quinoxalines,[23] or (tetrahydro)quinolines.[7g] In addition, the dehydrogenative reaction of ureas with alcohols has been described with a $[Ru(OH)_x/TiO_2]$ material, although affording only tertiary amines.[24] Therefore, the development of a protocol employing a stable and reusable heterogeneous material to obtain imidazolones from ureas and 1,2-diols is still a point of interest in synthetic and catalytic fields. To succeed in this goal, a material able to catalyze both dehydrogenation and condensation steps should be designed. In this direction, combining transition metal nanoparticles, known to be active in dehydrogenative processes, with inorganic metal oxide supports, having suitable acid−base properties, is a feasible approach to this problem. Here, we describe the first heterogeneously catalyzed protocol to perform the efficient and straightforward synthesis of imidazolones from ureas and 1,2-diols (including ethylene glycol) using a $[Pd/Al_2O_3]$ nanomaterial as a reusable catalyst (Scheme 1C).

RESULTS AND DISCUSSION

As a starting point of our investigation, a variety of solid nanomaterials composed of metal nanoparticles supported over γ-Al_2O_3 were prepared and tested in the reaction between *N*,*N*′-dicyclohexylurea **1** and 3-butene-1,2-diol **2** (Table 1, entries 2−9). Alumina was selected due to its demonstrated suitability to act as a metal nanoparticle support in dehydrogenation reactions.[7c,g,25] Among the tested materials, those presenting Pd, Pt, and Ru nanoparticles afforded imidazolone **3** in good to excellent yields (Table 1, entries 7−9), the Pd-nanostructured material being the one that yielded the best results. Moreover, $[Pd/Al_2O_3]$ also showed excellent activities when it was tested without being subjected to a hydrogenating pretreatment before reaction (Table 1, entry 10), unlike the Pt material whose activity decreased significantly when it was not reduced (Table S1, entry 8).

https://doi.org/10.1021/acscatal.2c01423
ACS Catal. 2022, 12, 6906−6922

Scheme 1. Examples of Dehydrogenative Condensations between Ureas and 1,2-Diols[a]

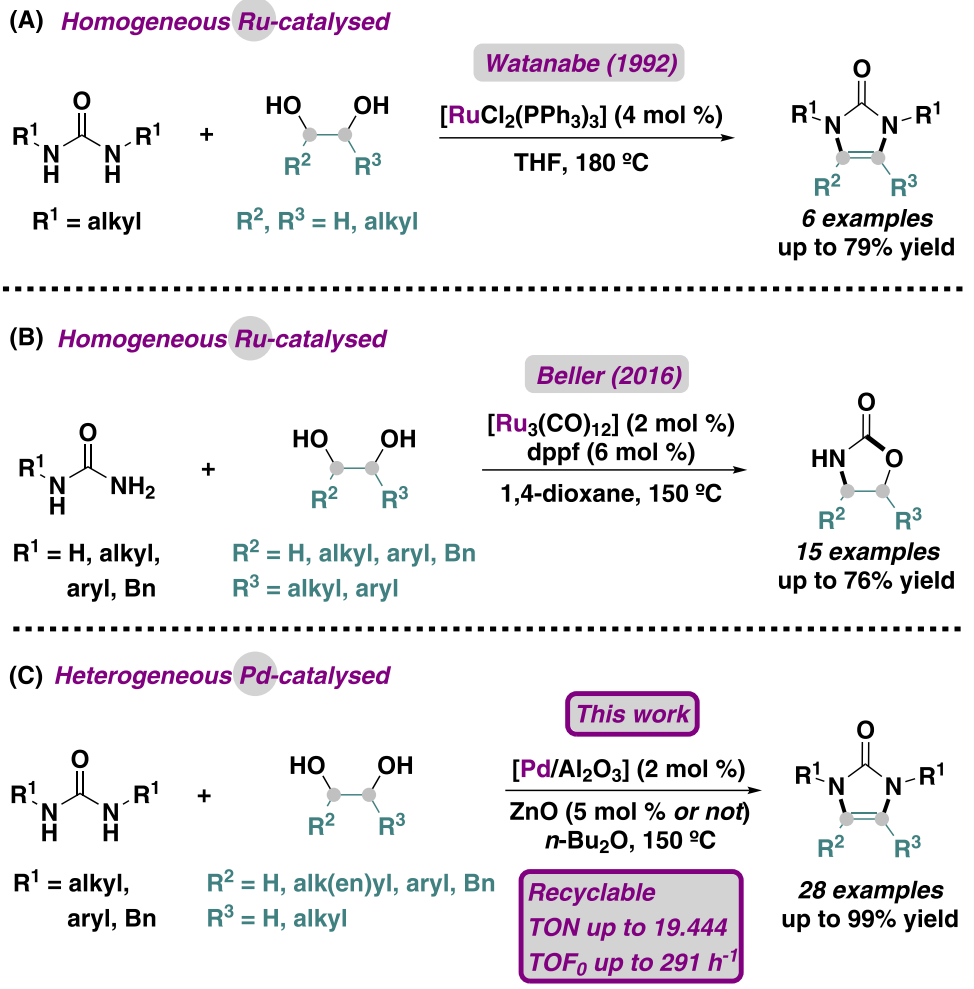

[a](A) Ru homogeneously catalyzed acceptorless dehydrogenation to afford imidazolones, as reported by Watanabe and co-workers; (B) Ru homogeneously catalyzed hydrogen-borrowing to yield oxazolidones, as reported by Beller and co-workers; (C) Pd heterogeneously catalyzed acceptorless dehydrogenation to yield imidazolones, as reported in this work. Bn = benzyl, dppf = 1,1′-ferrocenediyl-bis(diphenylphosphine).

Hence, we selected the [Pd/Al_2O_3] material to continue our study. Different reaction parameters were studied, and it was determined that an initial concentration of urea **1** between 0.5 and 0.75 M (Table S2, entries 4 and 5) and 150 °C (Table S3, entry 5) afforded excellent yields of imidazolone **3**. In addition, the influence of the solvent on the reaction was explored, and the best results were observed when employing dibutyl ether or *o*-xylene as solvents (Table S4, entries 6 and 7). Regarding the catalyst amount, good yields of **3** were obtained with a mol % of Pd larger than 0.5 (80%, Table 1, entry 11, and Table S5), 2 mol % being the optimum catalyst amount affording imidazolone **3** in 90% yield (Table 1, entry 9). Gratifyingly, the [Pd/Al_2O_3] system reached a TON value of 19444 when the reaction was performed at 0.05 mol % Pd for 90 h (Table 1, entry 14) and an initial turnover frequency (TOF_0) value of 291 h^{-1} at 0.5 mol % Pd (Table 1, entry 11). Moreover, [Pd/Al_2O_3] was compared with the [$RuCl_2(PPh_3)_2$] complex, described by the group of Watanabe for the synthesis of imidazolones from ureas and 1,2-diols.[3d] Although the Ru complex afforded imidazolone **3** in good yields, [Pd/Al_2O_3] showed better initial rates and TON and TOF_0 values (Table 1, entry 15, and Figure S1E). In addition, commercially available palladium-based materials such as [Pd/Al_2O_3] and [Pd/C] were tested under optimized reaction conditions (Table 1, entries 16 and 17, and Figure S1C,D) and were demonstrated to be less active than our [Pd/Al_2O_3] nanomaterial.

With the aim of better understanding the [Pd/Al_2O_3]-catalyzed dehydrogenative condensation of urea **1** and 1,2-diol **2**, kinetic and mechanistic studies were performed. Thus, it was determined that the reaction follows the first order for urea **1**, diol **2**, and the Pd catalyst (Figure S2). The reduction of the alkene moiety in imidazolone **3** pointed out a dehydrogenative mechanism, with the concomitant formation of H_2. This assumption was confirmed by the H_2 detection in the reaction between *N*,*N*′-dicyclohexylurea **1** and 1-phenylethane-1,2-diol **S11** (Figure S3). Moreover, the initial formation rate and yield of **3** did not show significant changes when the reaction was conducted in an inert atmosphere versus in air, whereas the yield of **3** was lower under O_2 conditions (Table S6). The good tolerance of the reaction to be conducted under air conditions is a remarkable advantage. With this information in hand, it can be deduced that the reaction proceeds through two steps: the first dehydrogenation of 3-butene-1,2-diol **2** to 1-hydroxybutan-2-one **4** catalyzed by Pd, followed by a condensation of 1-hydroxybutan-2-one **4** with *N*,*N*′-dicyclo-

https://doi.org/10.1021/acscatal.2c01423
ACS Catal. 2022, 12, 6906−6922

Table 1. Metal-Catalyzed Synthesis of Imidazolone 3 by a Dehydrogenative Condensation between Urea 1 and Diol 2

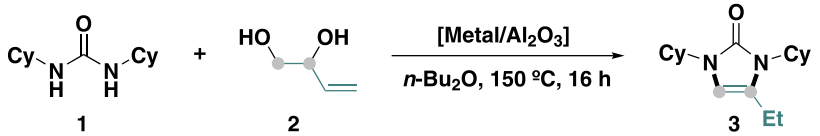

1 2 3

entry[a]	[cat.] (mol %)	3 (%)[b]	r_0 3 (%/h)[b]	TON[c]	TOF_0 (h^{-1})[d]
1	-	0	nd	nd	nd
2	[Fe/Al_2O_3] (2)	0	nd	nd	nd
3	[Co/Al_2O_3] (2)	1	nd	nd	nd
4	[Ni/Al_2O_3] (2)	0	nd	nd	nd
5	[Zn/Al_2O_3] (2)	0	nd	nd	nd
6	[Ag/Al_2O_3] (2)	7	nd	nd	nd
7	[Ru/Al_2O_3] (2)	44	nd	nd	nd
8	[Pt/Al_2O_3] (2)	78	nd	nd	nd
9	**[Pd/Al_2O_3] (2)**	**90**	**27.5**	**633**	**194**
10[e]	[Pd/Al_2O_3] (2)	86	21.0	nd	nd
11	**[Pd/Al_2O_3] (0.5)**	**80**	**10.5**	**2222**	**291**
12	[Pd/Al_2O_3] (0.25)	61	3.3	3389	183
13	[Pd/Al_2O_3] (0.05)	33	nd	9167	nd
14[f]	**[Pd/Al_2O_3] (0.05)**	**70**	**nd**	**19 444**	**nd**
15	[$RuCl_2(PPh_3)_2$] (2)	71	14.2	36	7
16[g]	[Pd/Al_2O_3]-ca. (2)	62	6.3	nd	nd
17[h]	[Pd/C]-ca. (2)	16	26.7	nd	nd

[a]Standard reaction conditions: *N,N′*-dicyclohexylurea **1** (112.17 mg, 0.5 mmol), 3,4-dihydroxy-1-butene **2** (84 μL, 1 mmol, 2 equiv), [metal/support] or complex (0.01 mmol, 2 mol %), and *n*-Bu_2O (1 mL) at 150 °C for 16 h. [b]Yield of **3** and initial reaction rates (r_0) were calculated by gas chromatography (GC) using *n*-dodecane as an internal standard. [c]Yield per mol % Pd on the surface (calculated by CO chemisorption). [d]Initial reaction rate per mol % Pd on the surface (calculated by CO chemisorption). [e]Reaction run with an unreduced material. [f]Run for 90 h. [g][Pd/Al_2O_3]-ca. stands for a commercially available Pd/Al_2O_3 material with 5 wt % reduced under H_2 at 200 °C for 2 h. [h][Pd/C]-ca. stands for a commercially available Pd/C material with 5 wt % reduced under H_2 at 200 °C for 2 h. nd = not determined.

Table 2. Textural and Physicochemical Properties of Pd-Supported Materials[a]

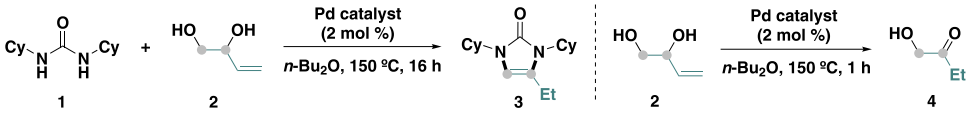

1 2 3 2 4

entry[b]	catalyst	BET (m^2/g)[c]	Pd part. size (nm)[d]	acid site density (μmol/g)[e]	3 (%)[f]	r_0 3 (%/h)[f]	4 (%)[f]	r_0 4 (%/h)[f]
1	[Pd/CaO]	42	3.2	6	51	6.8	5	6.0
2	[Pd/MgO]	5	2.6	7	49	10.6	4	4.3
3	[Pd/SiO_2]	280	4.6	30	52	8.3	33	32.0
4	[Pd/ZrO_2]	69	2.8	107	54	7.6	8	72.0
5	[Pd/TiO_2]	42	2.5	127	65	8.3	15	48.6
6	[Pd/Al_2O_3]	180/210[g]	2.8	200/232[h]	90	27.5	32	76.7
7	[Pd/Al_2O_3-1%]	209	2.5	162	71	21.0	16	36.3
8	[Pd/Al_2O_3-10%]	125	4.2	193	77	14.0	25	43.8
9	[Pd/Al_2O_3-10 °C/min]	178	5.1	107	78	12.5	27	45.6
10	[Pd/Al_2O_3-30 °C/min]	170	4.7	197	75	10.8	27	27.7
11	[Pd/Al_2O_3-300 °C]	160	2.3	223	75	14.5	21	65.9
12	[Pd/Al_2O_3-600 °C]	183	14.4	67	59	9.3	7	8.4

[a]Yield and initial rates of their catalytic activity in the dehydrogenative condensation between **1** and **2** and dehydrogenation of **2**. [b]Standard reaction conditions for 1,3-dicyclohexyl-4-ethyl-1,3-dihydro-2*H*-imidazol-2-one **3**: *N,N′*-dicyclohexylurea **1** (112.17 mg, 0.5 mmol), 3,4-dihydroxy-1-butene **2** (84 μL, 1 mmol, 2 equiv), Pd catalyst (21.3 mg, 0.01 mmol, 2 mol %), and *n*-Bu_2O (1 mL) at 150 °C for 16 h. Standard reaction conditions for 1-hydroxybutan-2-one **4**: 3,4-dihydroxy-1-butene **2** (84 μL, 1 mmol), Pd catalyst (21.3 mg, 0.01 mmol, 1 mol %), and *n*-Bu_2O (1 mL) at 150 °C for 1 h. [c]Values calculated from N_2 adsorption isotherms (Brunauer–Emmett–Teller, BET method). [d]Average diameter of Pd nanoparticles calculated from scanning transmission electron microscopy (STEM) measurements. [e]Total amount of NH_3 adsorbed by the catalyst determined through temperature-programmed desorption (TPD)-NH_3. [f]Yields of **3** and **4** and initial reaction rates were calculated by GC using *n*-dodecane as an internal standard. [g]BET of γ-Al_2O_3. [h]Total amount of NH_3 adsorbed by γ-Al_2O_3 determined through TPD-NH_3.

hexylurea **1** to afford imidazolone **3**. To determine the rate-limiting step of the whole process, we studied kinetically the dehydrogenation of 3-butene-1,2-diol **2** to 1-hydroxybutan-2-one **4** catalyzed by [Pd/Al_2O_3] as well as the condensation between *N,N′*-dicyclohexylurea **1** and 1-hydroxybutan-2-one **4** in the presence of [Pd/Al_2O_3]. Interestingly, we could measure an initial rate of 76.6%/h for the dehydrogenation process (Table 2, entry 6), whereas the condensation showed a rate of

https://doi.org/10.1021/acscatal.2c01423
ACS Catal. 2022, 12, 6906−6922

23.7%/h (Scheme S1C), much more similar to the rate of the global reaction (27.5%/h). Hence, it can be concluded that the condensation is the rate-limiting step of the process. Control experiments of the condensation reaction in the absence of the catalyst or with only calcined γ-Al_2O_3 demonstrated that this step is accelerated in the presence of the γ-Al_2O_3 support (Scheme S1).

The significant relevance of Al_2O_3 in both dehydrogenation[26] and condensation steps encouraged us to study the influence of other metal oxides as supports able to stabilize palladium nanoaggregates. Thus, the corresponding [Pd/CaO], [Pd/MgO], [Pd/SiO_2], [Pd/ZrO_2], and [Pd/TiO_2] nanostructured materials were prepared and tested in the dehydrogenative condensation between urea **1** and 1,2-diol **2** (Table 2, entries 1−6). All of the materials afforded imidazolone **3** in moderate yields (49−61%) and with lower initial rates than [Pd/Al_2O_3] (Table 2, entries 1−6). Dehydrogenation and condensation steps were studied independently for all of the Pd materials, revealing that [Pd/Al_2O_3] is the most active catalyst in terms of the initial rate for both steps (Table 2, entries 1−6, and Table S7). Condensation reactions are usually catalyzed in acidic or basic media. In addition, it has been reported that dehydrogenation reactions catalyzed by metal nanoparticles over metal oxide supports are strongly influenced by the acid−base properties of the support.[25a,c,f,27] Thus, acidic properties of the materials were evaluated by temperature-programmed desorption of ammonia (TPD-NH_3), which enabled us to quantify the acid site density and determine their strength (Table 2 and Figure S24). [Pd/CaO] and [Pd/MgO], considered as basic materials, barely presented acid sites. In contrast, for the other materials, acid sites were detected and quantified in the following order: [Pd/Al_2O_3] > [Pd/TiO_2] > [Pd/ZrO_2] > [Pd/SiO_2]. In all of the cases, the TPD-NH_3 profiles showed a maximum at a temperature between 193 and 196 °C, associated with weak acid sites.[28] Interestingly, calcined γ-Al_2O_3 showed a slightly higher number of acid sites than [Pd/Al_2O_3] (Table 2, entry 6), with maximums at 234, 405, and 632 °C associated with the weak, medium, and strong sites, respectively (Figure S24H). In addition, TPD-CO_2 experiments of [Pd/Al_2O_3] and γ-Al_2O_3 were performed, and basic sites were determined to be significantly inferior to acid sites for these materials (70 and 12 μmol/g for γ-Al_2O_3 and [Pd/Al_2O_3], respectively). An analysis of these TPD-CO_2 profiles reveals for [Pd/Al_2O_3] maximums at 101, 209, and 689 °C associated with the weak, medium, and strong sites, respectively, whereas γ-Al_2O_3 only displays maximums correlated to weak and strong sites (101 and 689 °C) (Fig. S26). The relationships between the number of acid sites and the initial rates of dehydrogenative condensation between urea **1** and 1,2-diol **2**, dehydrogenation of 1,2-diol **2**, and condensation between urea **1** and ketoalcohol **4** were considered (Figure 2). Although, in all of the cases, a maximum is observed for the most acidic material [Pd/Al_2O_3], dehydrogenation appears to be the transformation whose initial rate has a more linear relationship with the number of acid sites in the material.

At this point, several modifications in the [Pd/Al_2O_3] synthesis were explored. The corresponding materials with variations in the palladium loading (1 and 10 wt %, instead of 5 wt %), the calcination ramp (10 and 30 °C/min, instead of 1 °C/min), and the calcination temperature (300 and 600 °C, instead of 450 °C) were prepared and evaluated in the dehydrogenative condensation between urea **1** and 1,2-diol **2** as well as in the dehydrogenation of 1,2-diol **2** (Table 2, entries 7−12). All of the studied nanomaterials were shown to be less active than the originally prepared [Pd/Al_2O_3] for both dehydrogenative condensation and dehydrogenation. TPD-NH_3 experiments of these materials showed maximums

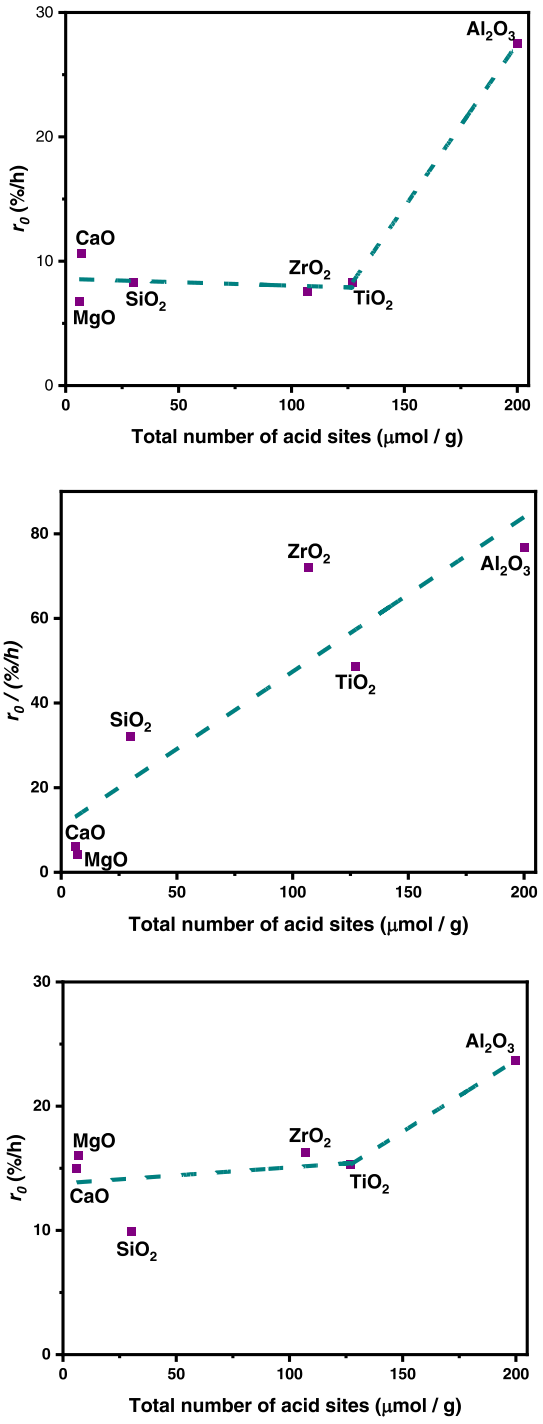

Figure 2. Initial rates (r_0) vs the total number of acid sites for Pd-supported catalysts in the dehydrogenative cyclization between urea **1** and diol **2** to yield imidazol-2-one **3** (top), the dehydrogenation of diol **2** to ketoalcohol **4** (middle), and condensation between urea **1** and ketoalcohol **4** (bottom). Standard reaction conditions: *N*,*N*′-dicyclohexylurea **1** (0−0.5 mmol), 3,4-dihydroxy-1-butene **2** (0−1 mmol) or 1-hydroxybutan-2-one **4** (0−1 mmol), [Pd/support] material (2 mol %), *n*-dodecane (0.26 mmol) as an internal standard, and *n*-Bu_2O (1 mL) at 150 °C.

https://doi.org/10.1021/acscatal.2c01423
ACS Catal. 2022, 12, 6906−6922

between 180 and 208 °C, which are characteristic of weak acid sites (Figure S25). In addition, acid site densities were significantly lower for [Pd/Al_2O_3-10 °C/min] and [Pd/Al_2O_3-600 °C] (Table 2, entries 9 and 12).

To understand the structural features of [Pd/Al_2O_3] that confer this material with such a high activity in the synthesis of imidazolone **3**, a detailed characterization was performed. Moreover, to identify the structural aspects that are more relevant to the good catalytic activity of [Pd/Al_2O_3], other palladium materials were also characterized by some of the techniques. Surface areas of all of the materials were determined (Table 2), with [Pd/Al_2O_3] and [Pd/SiO_2] materials being the ones with larger areas.

The X-ray diffraction (XRD) pattern of [Pd/Al_2O_3] (Figure 3, top) shows peaks at 2θ values of 39.9, 46.3, 67.8, 81.9, and

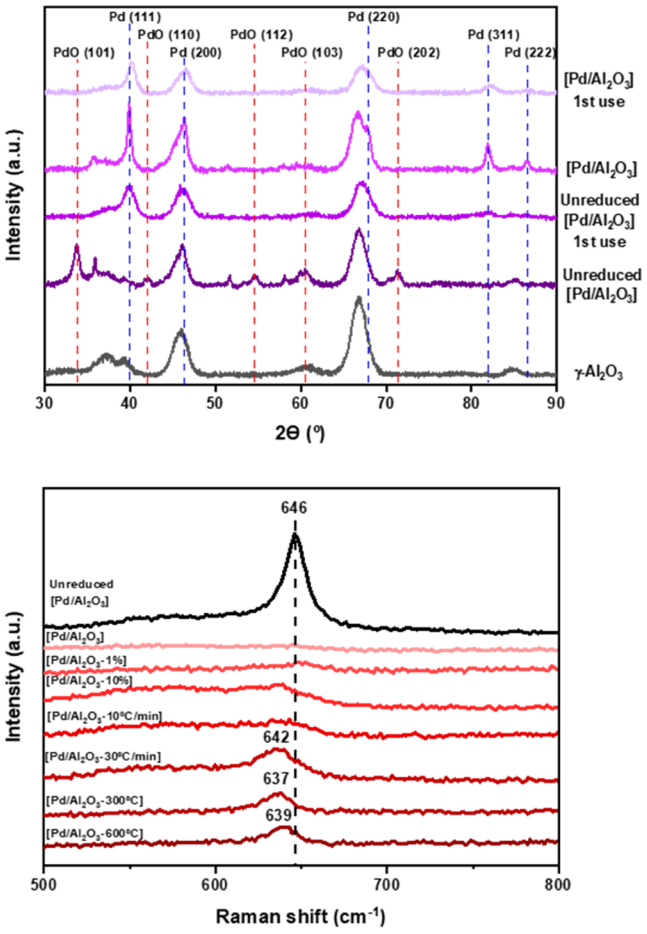

Figure 3. Top: X-ray diffraction patterns of γ-Al_2O_3 and [Pd/Al_2O_3] materials; the diffraction planes of Pd and PdO have been assigned. Bottom: Raman spectra of [Pd/Al_2O_3] materials.

86.4° corresponding to (111), (200), (220), (311), and (222) planes, respectively, of metallic Pd in a cubic close-packed structure (JCPDS card no 00-046-1043). In contrast, unreduced [Pd/Al_2O_3] shows peaks at values of 33.8, 42.2, 54.6, 60.5, and 71.4° corresponding to the planes (101), (110), (112), (103), and (202), respectively, of tetragonal PdO (JCPDS card no 00-041-1107) (Figure 3, top). It is interesting to note that when [Pd/Al_2O_3] was employed as the catalyst without previous reduction, the resulting material after reaction showed an XRD pattern similar to that of reduced [Pd/Al_2O_3]. Hence, this enables us to deduce that PdO crystallites detected by XRD, typically those larger than 4−5 nm, are reduced under the reaction conditions. In both unreduced and reduced [Pd/Al_2O_3] materials, peak shapes are either broad or show broader tails and narrower tips, suggesting the presence of small crystallites or a mixture of different crystallite sizes.[29] Characteristic Pd and PdO peaks were detected in all of the Pd materials, reduced or without reduction treatment (Figures S10 and S12), with the exception of [Pd/Al_2O_3-1%], which showed only the peaks of γ-Al_2O_3 (Figure S12A). In contrast, [Pd/Al_2O_3-10%], [Pd/Al_2O_3-10 °C/min], [Pd/Al_2O_3-30 °C/min], and [Pd/Al_2O_3-600 °C] (Figure S12B−D,F) showed narrower peaks, suggesting the presence of larger Pd crystallites.

To further explore materials' structure and determine Pd nanoparticle sizes, the materials were examined by high-angle annular dark-field−high-resolution scanning transmission electron microscopy (HAADF−HRSTEM) (Figures 4, S17, and S18). Average particle sizes of 3.0 and 2.8 nm were measured for unreduced and reduced [Pd/Al_2O_3] materials, respectively. The Pd materials with supports other than γ-Al_2O_3 showed average particle sizes of around 3 nm, with the exception of [Pd/SiO_2] in which a medium size of 4.6 nm was measured (Table 2 and Figure S17). In the case of materials based on Pd nanoparticles over γ-Al_2O_3, a larger average Pd nanoparticle size was confirmed in materials prepared with higher Pd loadings (10 wt %), at higher calcination temperatures (600 °C), or in faster calcination ramps (10 and 30 °C/min). A uniform distribution of Pd in [Pd/Al_2O_3] could be confirmed by energy-dispersive X-ray (EDX) elemental analysis (Figures 4 and S20). In addition, high-resolution transmission electron microscopy (HR-TEM) images of [Pd/Al_2O_3] were also obtained (Figure S19).

At this point, it was interesting to investigate whether PdO particles with a size inferior to 4−5 nm were present in the reduced materials. To this end, Raman spectra of all of the reduced materials were registered and compared with the spectrum of unreduced [Pd/Al_2O_3]. Remarkably, the PdO peak at 646 cm^{-1} in the unreduced [Pd/Al_2O_3] completely disappeared after reduction (Figure 3, bottom).[30] [Pd/SiO_2] showed a peak at 637 cm^{-1}, suggesting the incomplete reduction of PdO in this material (Figure S14C). In the case of [Pd/TiO_2], signals at 511 and 636 can be assigned to TiO_2 (Figure S14F).[31] Regarding the other [Pd/Al_2O_3] materials, it is remarkable that [Pd/Al_2O_3-30 °C/min], [Pd/Al_2O_3-300 °C], and [Pd/Al_2O_3-600 °C] displayed signals at 642, 637, and 639 cm^{-1}, which suggests the presence of PdO particles in these reduced materials (Figure 3, bottom).

Complementarily, X-ray photoelectron spectroscopic (XPS) studies of unreduced and reduced [Pd/Al_2O_3] were performed (Figure 5). The Pd 3d spectrum of unreduced [Pd/Al_2O_3] could be deconvoluted into four peaks corresponding to two doublets: one at 337.2 eV ($3d_{5/2}$) and 342.5 eV ($3d_{3/2}$) belonging to Pd(0) and the other at 338.9 eV ($3d_{5/2}$) and 344.5 eV ($3d_{3/2}$) belonging to Pd(II). In contrast, reduced [Pd/Al_2O_3] only showed a doublet at 336.9 eV ($3d_{5/2}$) and 342.0 eV ($3d_{3/2}$) assigned to Pd(0).

Finally, H_2-temperature-programmed reduction (TPR) studies of the Pd materials with different metal oxides as supports revealed the presence of two or more peaks at temperatures lower than 200 °C in all of the cases (Figure S23). In TPR studies, H_2 consumption at higher temperatures is associated with smaller-sized particles, due to stronger metal−support interactions.[28a,32] Thus, the presence of several

https://doi.org/10.1021/acscatal.2c01423
ACS Catal. 2022, 12, 6906−6922

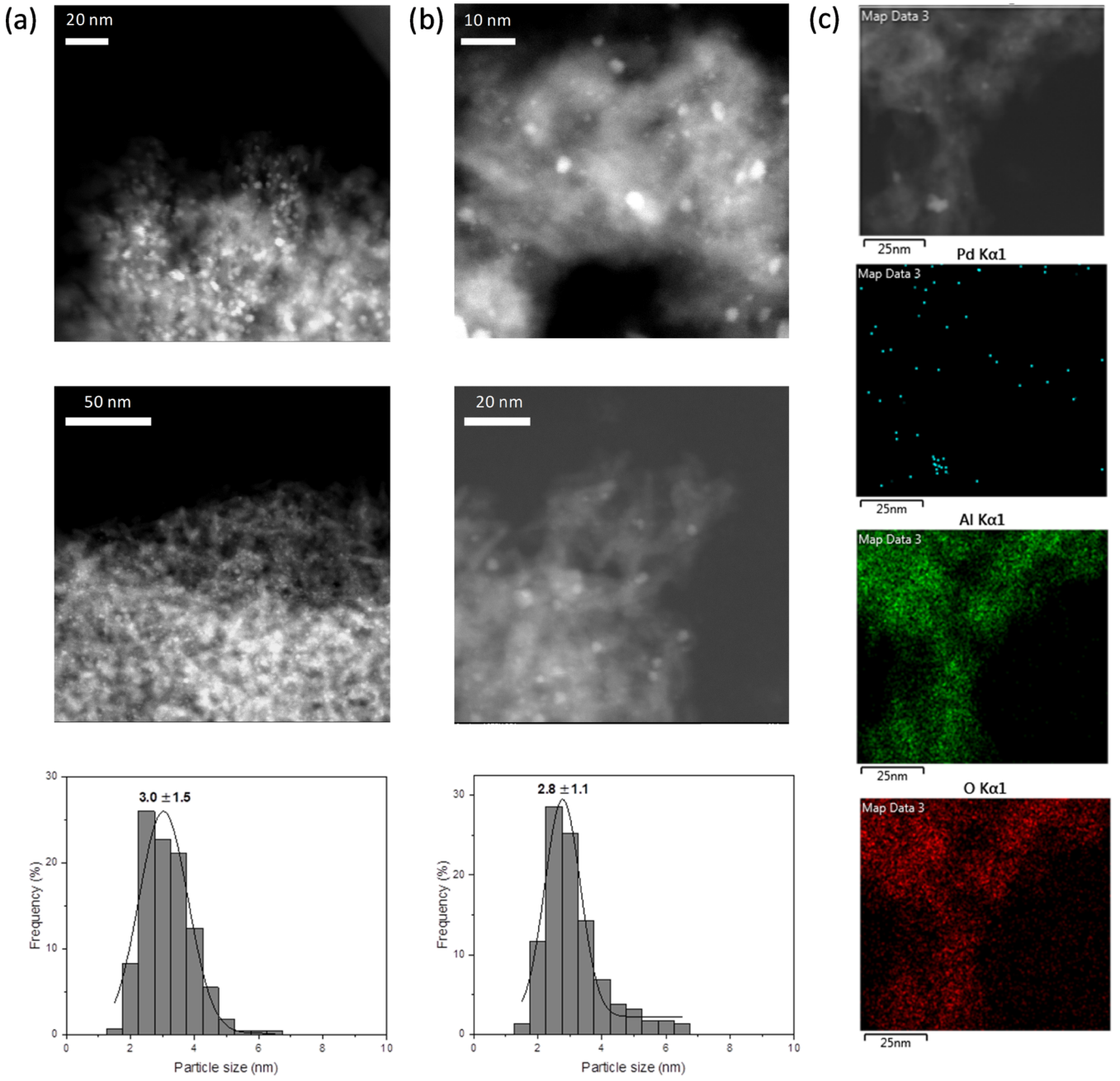

Figure 4. HAADF−HRSTEM images and Pd particle size distribution of unreduced [Pd/Al_2O_3] (a) and [Pd/Al_2O_3] (b) materials; EDX elemental mapping of Pd, Al, and O for [Pd/Al_2O_3] (c).

peaks confirms that the materials contain Pd nanoparticles of different sizes, as the XRD and STEM studies suggested. In addition, a maximum of low intensity between 311 and 409 °C was observed for most of the materials. H_2 consumption at temperatures of around 300 °C was attributed to the reduction of smaller PdO particles or the support.[28a] It is interesting to note that an important H_2 consumption between 336 and 409 °C was observed for [Pd/Al_2O_3-300 °C] containing a higher amount of smaller particles (Figure S23I). In the case of [Pd/MgO], an intense peak at 638 °C was detected corresponding to the formation of Mg_8H or Mg_8OH species (Figure S23B).[33] Remarkably, TPR profiles of [Pd/Al_2O_3] and [Pd/TiO_2] showed a negative peak at 72 °C (Figure S23F,G), indicating the release of H_2 after the reduction of bulk PdO at room temperature and the formation of β-PdH.[28a]

With all of this information in hand, it can be deduced that the material composed of Pd(0) nanoparticles of several sizes (2.8 nm average) over the acidic γ-Al_2O_3 is the optimum catalyst for dehydrogenative condensation between urea **1** and 1,2-diol **2**.

Then, the heterogeneous nature of the catalysis was proved by performing a hot filtration test (Figure S5). In addition, inductively coupled plasma (ICP) measurements of the reaction mixture and [Pd/Al_2O_3] after reaction also demonstrated that Pd leaching did not occur under the reaction conditions (Pd content measured by ICP: fresh catalyst, 5.3 wt %; used catalyst, 5.1 wt %; and Pd in solution, 0.004 mg; see Supporting Information, SI, Section S6.2). Thus, the reusability of the material was studied with unreduced [Pd/Al_2O_3] for practical reasons. To our delight, the material could

https://doi.org/10.1021/acscatal.2c01423
ACS Catal. 2022, 12, 6906−6922

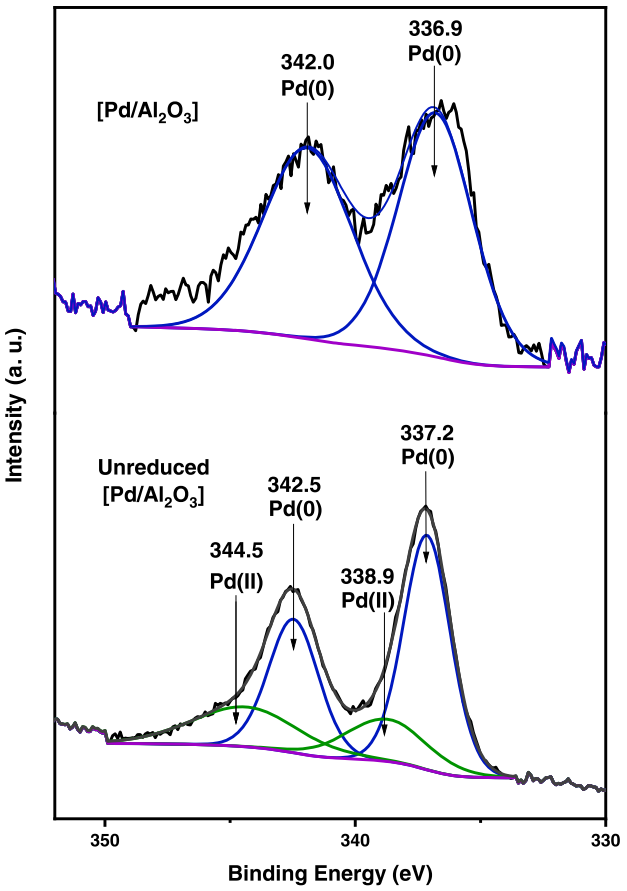

Figure 5. Pd 3d XPS spectra of $[Pd/Al_2O_3]$ materials.

be reused for six cycles, with a calcination treatment after each use to eliminate the deposition of organic compounds on the catalyst's surface, and without significant loss of its activity and selectivity (Figure 6; see SI for the experimental procedure). In fact, initial rates were determined for each use of the catalyst, confirming the good activity of the reused material. As commented before, the XRD pattern of unreduced $[Pd/Al_2O_3]$ after the first use showed typical peaks of Pd(0) (Figure 3, top). No significant changes were observed in the XRD of either the unreduced material after the sixth use or the reduced material after the first use (Figure 3, top and Figure S11). In contrast, XPS studies of reduced $[Pd/Al_2O_3]$ after the first use showed a Pd 3d spectrum that could be deconvoluted into two doublets, indicating the presence of mainly Pd(0) and some amount of PdO in this material (Figure S16C). Moreover, BE values of Pd(0) and PdO in the used material appeared at lower eV values, suggesting the presence of larger Pd nanoparticles.[28a,34] In fact, HAADF−HRSTEM studies of unreduced $[Pd/Al_2O_3]$ after the first and sixth uses showed a significant increase in the average particle size (Figure S21). Despite the presence of larger particles, these materials also displayed Pd particles with a size <5 nm; thus, it is not possible to determine whether the catalytic activity corresponds to a specific Pd particle size or to the presence of a wide variety of particles.

Once the reusability of the material was demonstrated, we decided to investigate its range of application for the synthesis of a variety of imidazolones. First, we studied the reactions of a variety of ureas with 1,2-diols bearing an alkenyl or phenyl group in the β position to one of the hydroxyl groups (Scheme 2). A wide range of imidazolones were obtained from 3-butene-1,2-diol **2** and *N*,*N*′-substituted ureas. *N*,*N*′-dialkyl-substituted ureas afforded the corresponding imidazolones **3**, **5**, and **6** in moderate to good yields (50−79%). To our delight,

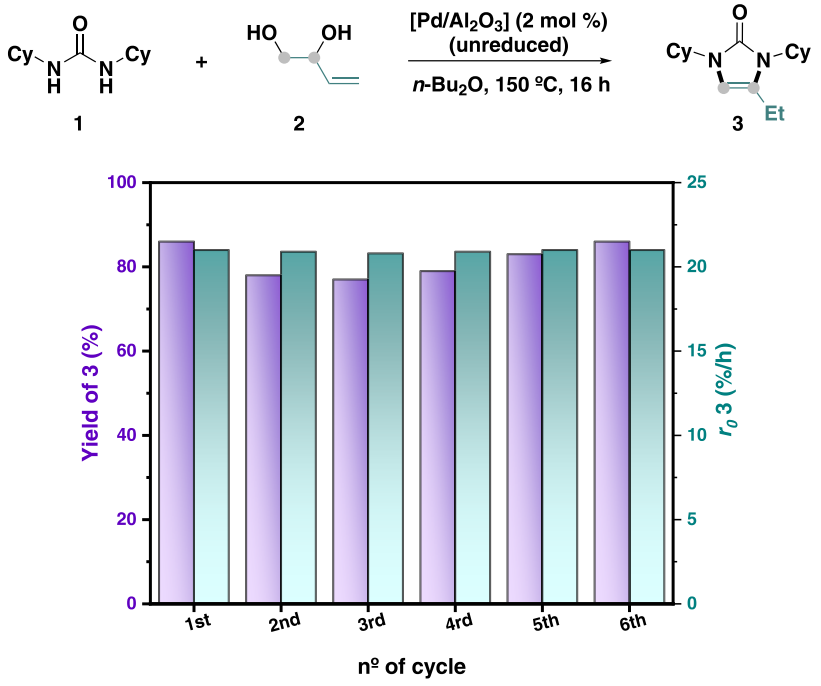

Figure 6. $[Pd/Al_2O_3]$ catalyst reuse for dehydrogenative cyclization of urea **1** and diol **2** to synthesize imidazol-2-one **3**. Standard reaction conditions: *N*,*N*′-dicyclohexylurea **1** (590.9 mg, 2.5 mmol), 3,4-dihydroxy-1-butene **2** (0.42 mL, 5 mmol, 2 equiv), $[Pd/Al_2O_3]$ (unreduced) (106.4 mg, 0.05 mmol, 2 mol %), *n*-dodecane (225 mg, 1.3 mmol) as an internal standard, and *n*-Bu_2O (5 mL) at 150 °C for 16 h.

https://doi.org/10.1021/acscatal.2c01423
ACS Catal. 2022, 12, 6906−6922

Scheme 2. [Pd/Al_2O_3]-Catalyzed Synthesis of Imidazol-2-ones from *N,N′*-Disubstituted Ureas and 3,4-Dihydroxy-1-butene (2) or 1-Aryl-1,2-ethanediols[a]

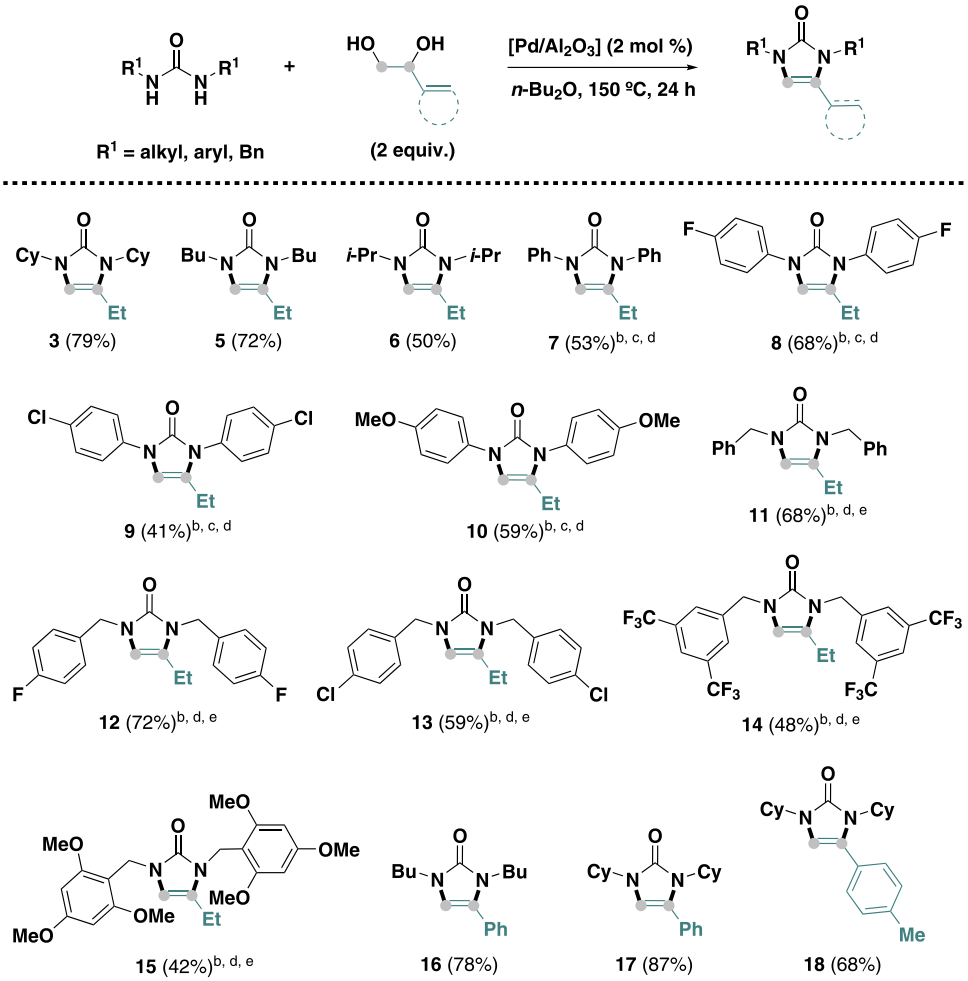

[a]Standard reaction conditions: *N,N′*-disubstituted urea (0.5 mmol), 1,2-diol (1 mmol, 2 equiv), [Pd/Al_2O_3] (2 mol % Pd, 21.3 mg), and *n*-Bu_2O (1 mL) at 150 °C for 24 h. Isolated yields after column chromatography on neutral alumina are given within parentheses. [b]Using *o*-xylene as the solvent. [c]Run for 16 h. [d]Traces of the corresponding mixture of oxazolones were detected. [e]Isolated yields after column chromatography on silica are given within parentheses. Bn = benzyl.

aryl-substituted ureas could also be employed in our protocol. Electron-donating as well as electron-withdrawing functionalities in arenes were well tolerated, and the corresponding imidazolones **7**−**10** could be isolated (41−68%). Moreover, *N,N′*-dibenzyl ureas were also explored as substrates for this reaction and successfully afforded the corresponding imidazolones **11**−**15** in moderate to good isolated yields (42−72%). In these cases, good tolerance to aromatic ring substituents was also observed, including F and CF_3 groups. For both aryl- and benzyl-substituted ureas, traces of the corresponding oxazolones were detected. In these cases, the reactions were performed using *o*-xylene instead of dibutyl ether as the solvent due to the better solubility of ureas and improved selectivities in this solvent. In addition, phenyl- and *o*-tolyl-substituted 1,2-diols were reacted with *N,N′*-dialkyl-substituted ureas, yielding the *N*-alkyl-substituted imidazolones **16**−**18** in good to excellent yields (68−87%).

However, when the dehydrogenative condensation between *N,N′*-dicyclohexylurea **1** and 1,2-pentanediol **19** was attempted under the typical reaction conditions, the corresponding imidazolone **20** was obtained in almost negligible yields (Figure 7 and Table S9). This result showed that our protocol was limited to the use of activated 1,2-diols. With the aim of achieving a more applicable method, we decided to explore the possibility of using ZnO as an additive, able to activate 1,2-diols.[7c,g,22,35] To our delight, the combination of [Pd/Al_2O_3] nanomaterial with small amounts of ZnO (5 mol %) resulted in an active catalytic system that afforded the corresponding imidazolone in high yield (Figure 7 and Table S9).

With this information in hand, the design of a material able to catalyze the acceptorless dehydrogenation of unactivated 1,2-diols and ureas was attempted. In this direction, we prepared a material based on Pd nanoparticles stabilized over a ZnO support. Furthermore, several bimetallic Pd−Zn-containing nanostructured materials using γ-Al_2O_3 as a solid matrix were also prepared. Gratifyingly, both [Pd/ZnO] and [Pd(5%)−Zn(5−10%)/Al_2O_3] materials were found to be active catalysts for the acceptorless dehydrogenative condensation between *N,N′*-dicyclohexylurea **1** and 1,2-pentanediol **19** (Figure 7 and Table S9). Pd−Zn nanomaterials have been intensively investigated in the past years due to their interesting applications in relevant processes such as CO_2 hydrogenation,[36] reforming/dehydrogenation of methanol,[37] semihydrogenation of alkynes,[38] etc. In these cases, the

https://doi.org/10.1021/acscatal.2c01423
ACS Catal. 2022, 12, 6906−6922

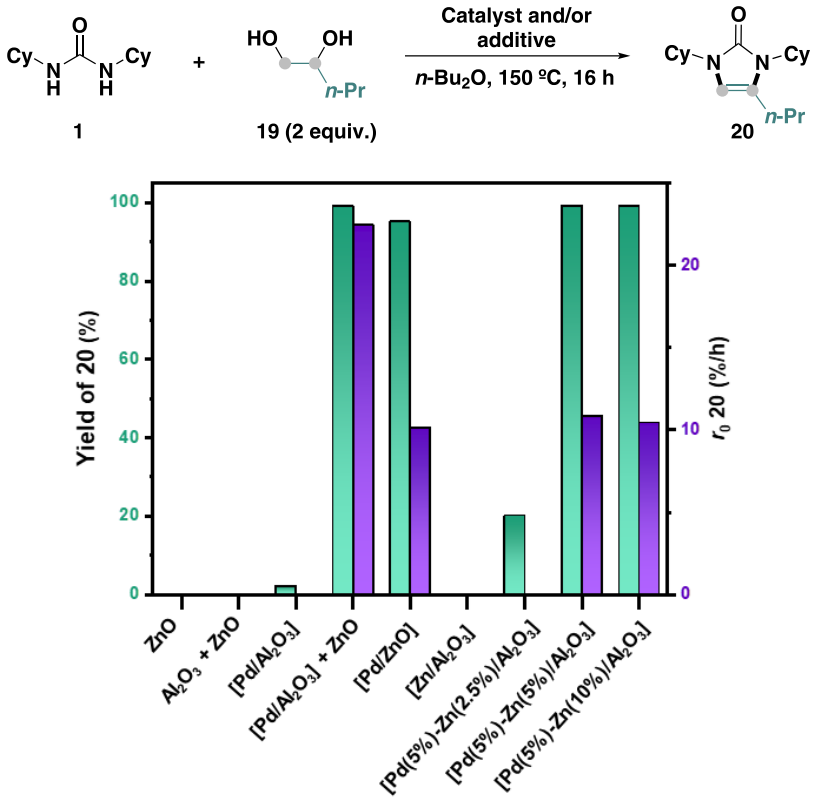

Figure 7. Study of the catalytic system for the acceptorless dehydrogenative condensation between *N*,*N*′-dicyclohexylurea **1** and 1,2-pentanediol **19**. Standard reaction conditions: *N*,*N*′-dicyclohexylurea **1** (112.17 mg, 0.5 mmol), 1,2-pentanediol **19** (107 μL, 1 mmol, 2 equiv), *n*-Bu_2O (1 mL), calcined γ-Al_2O_3 (21.3 mg) or the corresponding catalyst (0.01 mmol, 2 mol % Pd), and ZnO (2 mg, 0.025 mmol, 5 mol %) when indicated at 150 °C for 16 h. The yield of **20** and initial reaction rates were calculated by GC using *n*-dodecane as an internal standard.

formation of Pd−Zn alloys has been reported in materials where Pd nanoaggregates are supported over a ZnO matrix, as well as in the case of materials based on Pd−Zn bimetallic species over different metal oxide supports.

To gain further insights into the structure of our materials, [Pd/ZnO] and [Pd(5%)−Zn(5%)/Al_2O_3] were characterized. The BET surface areas were determined to be 18 m^2/g for [Pd/ZnO] and 164 m^2/g for [Pd(5%)−Zn(5%)/Al_2O_3]. In addition, TPD-NH_3 studies of [Pd(5%)−Zn(5%)/Al_2O_3] showed an acid site density of 141 μmol/g, whereas the density determined for [Pd/ZnO] was 49 μmol/g, significantly lower than that of [Pd/Al_2O_3] (200 μmol/g) (Figures S24D and S25G). These materials showed the main NH_3 desorption peak at temperatures between 159 and 180 °C, values generally associated with weak acid sites. Interestingly, the presence of two other peaks at 424−449 °C and 621−626 °C was also detected, indicating the coexistence of other types of acid sites in these materials.

XRD patterns of the two materials showed the characteristic peaks of tetragonal PdO crystallites in the case of materials before reduction and the peaks of the metallic Pd in a cubic close-packed structure for materials after reduction (Figures S10D and S12G). In addition, [Pd/ZnO] showed two peaks at 42.3 and 44.1° that were assigned to the reflection of the (111) and (200) β-Pd−Zn alloy crystal planes, respectively (Figure S13).[36,37a,38b] For [Pd(5%)−Zn(5%)/Al_2O_3] material, the peak corresponding to the (111) plane of the alloy was observed, whereas the peak corresponding to the (200) plane is overlapped with γ-Al_2O_3 reflections (Figure S13). In all of the cases, broad peak shapes were observed, suggesting the presence of small nanoparticles. With the aim of confirming this observation, the materials were examined by HAADF−HRSTEM (Figures S17D and S22A). An average particle size of 2.9 nm was measured for [Pd/ZnO] (Figure S17D), whereas a larger particle size of 5.8 nm was detected for [Pd(5%)−Zn(5%)/Al_2O_3] (Figure S22A). Raman spectra of the materials were also registered, and the absence of PdO particles with a size <4−5 nm was confirmed (Figures S14D and S15). Energy-dispersive X-ray (EDX) experiments of [Pd(5%)−Zn(5%)/Al_2O_3] were performed, confirming the good dispersion and intimate contact of both metal centers (Figure S22B−D). Temperature-programmed reduction experiments showed for both materials a main peak at temperatures between 75 and 79 °C assigned to the main Pd nanoparticles as well as a peak at higher temperatures between 278 and 358 °C that could belong to the reduction of smaller nanoparticles, the corresponding support, or the alloy formation[37a] (Figure S23D,H). To further investigate the possible formation of a Pd−Zn alloy, XPS analysis of [Pd(5%)−Zn(5%)/Al_2O_3] was performed (Figure S16D,E). The Pd 3d signal can be deconvoluted into two main peaks at 334.8 eV ($3d_{5/2}$) and 340.2 eV ($3d_{3/2}$) assigned to Pd(0), similar to those recorded for [Pd/Al_2O_3], but at slightly lower eV values, which agree with a larger particle size.[28a,34] In addition, Pd 3d spectra of [Pd(5%)−Zn(5%)/Al_2O_3] show another doublet at higher BE values (336.1 and 342.3 eV) that was assigned to the formation of a Pd−Zn alloy.[36,37,38a] Moreover, the alloy formation is further supported by the observation of a shoulder (1013.7 eV) ascribed to the peak of

https://doi.org/10.1021/acscatal.2c01423
ACS Catal. 2022, 12, 6906−6922

Scheme 3. [Pd/Al_2O_3]-Catalyzed Synthesis of Imidazol-2-ones from *N,N′*-Dialkyl Ureas and Alkyl or Benzyl-1,2-diols[a]

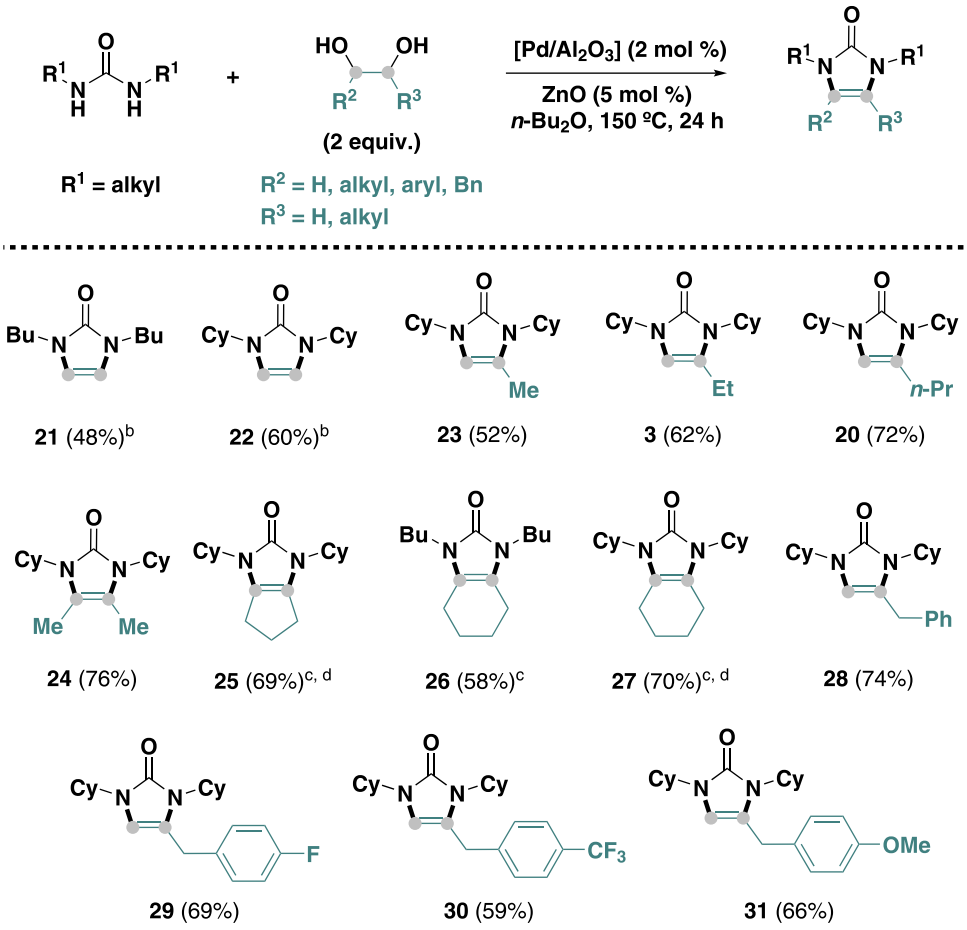

[a]Standard reaction conditions: *N,N′*-dialkylurea (0.5 mmol), 1,2-diol (1 mmol, 2 equiv), [Pd/Al_2O_3] (2 mol % Pd, 21.3 mg), ZnO (5 mol %, 2 mg), and *n*-Bu_2O (1 mL) at 150 °C for 24 h. Isolated yields after column chromatography on neutral alumina are given within parentheses. [b]Run at 90 h. [c]Using [Pd/Al_2O_3] (5 mol % Pd). [d]ZnO (10 mol %) was added.

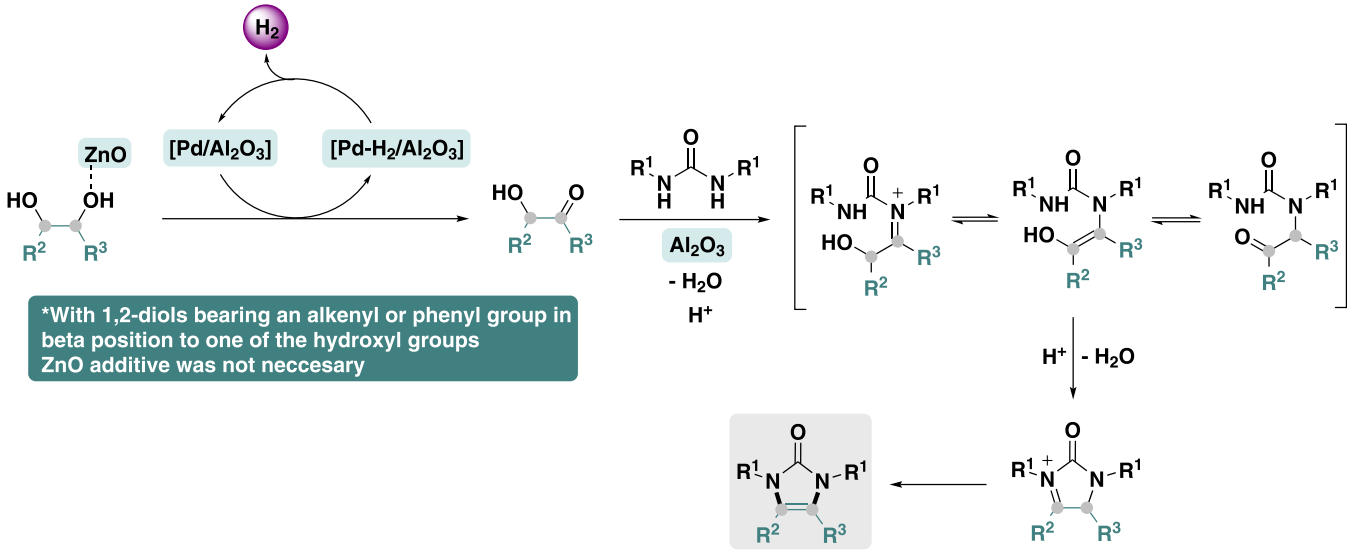

Figure 8. Proposed mechanism for the [Pd/Al_2O_3]−ZnO-catalyzed acceptorless dehydrogenation between ureas and 1,2-diols to afford imidazolones.

ZnO (1023.0 eV) in the Zn LMM Auger spectra, which was assigned to metallic zinc.[36b,37a]

Initial rates of the acceptorless dehydrogenative condensation between urea **1** and 1,2-pentanediol **19** were evaluated for the three types of catalytic systems, and it was determined that

https://doi.org/10.1021/acscatal.2c01423
ACS Catal. 2022, 12, 6906−6922

the [Pd/Al_2O_3]−ZnO combination was the more active system. This fact can be related to the major accessibility of γ-Al_2O_3 in this material and the higher number of acid sites. The heterogeneous nature of the [Pd/Al_2O_3]−ZnO combination and [Pd(5%)−Zn(5%)/Al_2O_3] catalytic system was investigated. First, a hot filtration test was performed for both systems, and neither of them showed leaching of active metal species (Figures S8 and S9). Moreover, additional ICP measurements of [Pd/Al_2O_3]−ZnO and [Pd(5%)−Zn(5%)/Al_2O_3] materials after reaction and reaction waters further demonstrated the heterogeneity of the system (see SI, Section S7.3). Hence, reusing experiments were attempted for both catalytic systems. To our delight, both systems were demonstrated to be reusable in two catalytic cycles (Figures S6 and S7).

Once the feasibility of the dehydrogenation of unactivated diols using the Pd−Zn cooperative catalysis was demonstrated, we decided to evaluate the general applicability of the reaction with these kinds of substrates (Scheme 3). For practical reasons, and due to its good activity and stability, we performed this study with the [Pd/Al_2O_3]−ZnO catalytic system. Remarkably, employing this protocol, imidazolones **21** and **22** were obtained from the corresponding *N*,*N*′-dialkyl ureas and ethylene glycol in moderate yields (48−60%) over long reaction times. Other unactivated diols such as 1,2-propanediol, 1,2-butanediol, 1,2-pentanediol, and 2,3-butanediol also afforded the corresponding imidazolones **23**, **3**, **20**, and **24** in good yields (52−72%). Bicyclic imidazolones **25**, **26**, and **27** were successfully obtained (58−70%) from dialkyl ureas and cyclic 1,2-diols employing 5 mol % [Pd/Al_2O_3] and ZnO as the catalytic system. Finally, the acceptorless dehydrogenative condensation between *N*,*N*′-dicyclohexylurea 1 and several 3-phenylpropane-1,2-diols was explored. Gratifyingly, the corresponding imidazolones **28**−**31** were obtained in good to moderate yields (59−74%) and remarkable tolerance was exhibited to both electron-donating or electron-withdrawing substituents in the phenyl ring.

A reaction mechanism was proposed based on all of the performed experiments (Figure 8). First, a Pd-catalyzed dehydrogenation of the corresponding diol to the ketoalcohol takes place, with the concomitant formation of a Pd hydride species followed by H_2 generation (*vide supra*). This dehydrogenation is assisted by [Pd/Al_2O_3] acid sites.[26] In the case of unactivated diols, the presence of a Zn species is required for alcohol activation.[7c,g,22,35] For activated diols, such as 1-phenylethane-1,2-diol **S11**, able to react using [Pd/Al_2O_3] as the catalyst, control experiments showed that the dehydrogenation occurs in the α position with respect to the activating group (Scheme S2). Then, the first Al_2O_3-catalyzed condensation between the ketoalcohol and the urea is proposed to form an iminium cation. The equilibrium of this species with an enamine−enol compound and a carbonyl compound explains the second condensation that affords a five-membered cyclic compound. Finally, the cyclic iminium reorganizes to enamine to afford the final imidazolone. In the case of 1,2-diols with an alkene function in their structure, a double-bond hydrogenation is observed to take place. This is easily explained as a consequence of the large reducibility of alkenes in the presence of a Pd catalyst and the formed H_2. As demonstrated before, kinetic studies have shown that the rate-determining step of the reaction is the Al_2O_3-catalyzed condensation, in which Pd does not play a role. To gain further insights into this mechanism, kinetic experiments with several substituted phenylethane-1,2-diols were performed, and their normalized rates ($\log K_R/K_H$) were plotted against the corresponding Hammet constants (Table S8 and Figure S4).[39] If the rate-determining step of the reaction was the condensation, a linear relationship with a positive slope would be the expected result.[26] However, a more complex behavior was observed. More specifically, for electron-withdrawing substituents, a lack of sensitivity as well as very low rates were measured, whereas for electron-donating substituents, a positive slope was detected. This kind of complex behavior has been associated with changes in the rate-determining step in the function of the specific substrates.[40] In our case, a plausible explanation would be that the dehydrogenation of the corresponding 1,2-diol can be totally hampered in the presence of phenylethane diols with electron-withdrawing substituents, less prone to C−H activation.

CONCLUSIONS

To sum up, an efficient, robust, and reusable nanostructured solid catalytic system was developed for the synthesis of imidazolones from easily available ureas and 1,2-diols. A catalyst based on Pd nanoparticles stabilized over a γ-Al_2O_3 matrix, [Pd/Al_2O_3], was described for the first time as an active and selective material able to mediate the 1,2-diol dehydrogenation to a ketoalcohol followed by the first condensation, tautomeric equilibrium, and the second condensation to yield the corresponding imidazolone. This protocol has shown its applicability through the synthesis of a wide range of imidazolones (28 new molecules). With the aim to better understand this process and the key features of the active centers in the catalyst, several materials based on Pd nanoparticles over γ-Al_2O_3 and various metal oxide supports with different properties were obtained and compared catalytically and structurally (XRD, HR-TEM, STEM, EDX, Raman spectroscopy, TPR, TPD-NH_3, TPD-CO_2, XPS, and BET). These investigations allowed us to deduce that Pd nanoparticles with a wide range of sizes (2.8 nm medium size) stabilized onto a γ-Al_2O_3 support containing a large number of acid sites forms the ideal catalytic system. Kinetic studies have shown that the material's acidity has a larger impact on the dehydrogenation step than on the condensation step. In addition, γ-Al_2O_3 was demonstrated to be able to promote the condensation step. Furthermore, we were able to design and characterize several bimetallic Pd−Zn-based materials, [Pd/ZnO] and [Pd(5%)−Zn(5%)/Al_2O_3], for the acceptorless dehydrogenation of unactivated 1,2-diols. Finally, Pd−Zn was applied cooperatively, through the use of a catalytic system based on a [Pd/Al_2O_3]−ZnO composite, to the acceptorless dehydrogenative condensation between ureas and unactivated 1,2-diols, including ethylene glycol. Remarkably, [Pd/Al_2O_3], [Pd(5%)−Zn(5%)/Al_2O_3], and [Pd/Al_2O_3]−ZnO catalytic systems demonstrated robustness and reusability.

This work identifies the first heterogeneous solid catalyst capable of performing the straightforward synthesis of imidazolones from ureas and 1,2-diols. In our opinion, the remarkable stability of the nanostructured catalyst presented here and the wide availability of the starting materials make this method an interesting alternative for accessing new imidazolone scaffolds in an atom-economical, practical, and more sustainable manner.

https://doi.org/10.1021/acscatal.2c01423
ACS Catal. 2022, 12, 6906−6922

EXPERIMENTAL SECTION

General Information. All unreduced and reduced catalysts were analyzed by X-ray powder diffraction (XRD) using a Cubix-Pro PANalytical diffractometer equipped with a detector PANalytical X'Celerator (Cu Kα radiation). The amount of Pd contained in the fresh and used catalysts was determined by inductively coupled plasma-optical emission spectroscopy (ICP) using Varian 715-ES after the dissolution of the solid samples in an HF/HNO_3/HCl aqueous solution (1:1:3 vol). Liquid nitrogen adsorption was analyzed using N_2 adsorption isotherms at −196 °C in a Micrometrics FlowSorb equipment. The specific surface areas of the reduced catalysts were calculated by applying the Brunauer−Emmett−Teller (BET) model over the range P/P^0 = 0.05−0.25 of the isotherms. Fresh and used catalysts were observed by STEM and TEM using a JOEL JEM 2100F electron microscope working at 200 kV. Temperature-programmed reduction with H_2 (H_2-TPR) experiments were carried out in Micrometrics Autochem 2910 equipped with a TCD detector, using 50 mg of freshly calcined catalyst and increasing the temperature from room temperature to 800 °C with a heating ramp of 10 °C/min under 10% H_2/Ar (vol %) and a constant flow rate of 50 mL/min. Ammonia thermoprogrammed desorption (NH_3-TPD) profiles were obtained after a previous pretreatment step of the previously calcined and reduced catalyst (100 mg, with a pellet size of 0.4−0.8 nm) under a He flow from room temperature to 450 °C; after cooling to 100 °C, adsorption of NH_3 was allowed at 100 °C, followed by a cleaning step using He flow to eliminate the physisorbed NH_3, and the thermoprogrammed desorption was carried out by heating the samples from 100 to 700 °C at a heating rate of 10 °C/min. The evolved NH_3 was analyzed using Micrometrics Autochem II equipped with a TCD detector connected online with an Omnistar mass spectrometer. CO_2 thermoprogrammed desorption (CO_2-TPD) profiles were obtained after a previous pretreatment step of the previously calcined and reduced catalyst (100 mg, with a pellet size of 0.4−0.8 nm) under a He flow from room temperature to 450 °C; after cooling to 50 °C, adsorption of CO_2 was allowed at 50 °C, followed by a cleaning step using He flow to eliminate the physisorbed CO_2, and the thermoprogrammed desorption was carried out by heating the samples from 50 to 800 °C at a heating rate of 10 °C/min. The evolved CO_2 was analyzed using Micrometrics Autochem II equipped with a TCD detector connected online with an Omnistar mass spectrometer. Pd metal dispersion of the samples was estimated from the CO adsorption using the double-isotherm method on a Quantachrome Autosorb-1C equipment. Prior to adsorption, the samples (300 mg, with a pellet size of 0.4−0.8 nm) were reduced in situ in flowing pure hydrogen at the same reduction temperature as that applied before catalysis (200 °C for 2 h and 3 °C/min). After reduction, the samples were degassed at 1333×10^{-3} Pa for 2 h at the reduction temperature, and then the temperature was lowered to 25 °C for 1 h. Then, pure CO was admitted and the first adsorption isotherm (i.e., the total CO uptake) was measured. After evacuation at 35 °C, the second isotherm (i.e., the reversible CO uptake) was measured. The amount of chemisorbed CO was calculated by subtracting the two isotherms. The pressure range studied was 0.511×10^4 Pa. The dispersion of Pd was calculated from the amount of irreversibly adsorbed CO assuming a stoichiometry of Pd/CO = 1. The Raman spectra of the power catalysts were analyzed using an excitation of 514 nm in a Renishaw inVia Raman spectrometer. The XPS spectra were recorded with a SPECS spectrometer equipped with a Phibos 150 MCD-9 multichannel analyzer, using a non-monochromatic Al K_α (1486.6 eV) X-ray source. The spectra were recorded with an X-ray power of 100 W, a pass energy of 30 eV, and under an operating pressure of 10^{-9} mbar. The XPS spectra were referenced to the C 1s peak (284.5 eV), and spectral processing was performed using the CASA XPS software.

General Procedure for Catalyst Preparation. [Pd/Al_2O_3] was prepared with 5 wt % Pd metal by impregnation of γ-Al_2O_3 (0.847 g) with a solution of K_2PdCl_4 (0.153 g, 0.47 mmol) in a mixture of water:acetone (1:8, 48 mL). The mixture was stirred for 16 h and then evaporated to dryness under vacuum at 40 °C. The resulting powder was calcined in a furnace in air with a heating ramp of 1 °C/min up to 450 °C and held at that temperature for 4 h to obtain the oxidized catalyst. The sample was activated before reaction by heating the solid powder in a stream of N_2 (100 mL/min) with a heating ramp of 2 °C/min to 200 °C; the material was held at 200 °C under H_2 for 2 h and then cooled down to room temperature under a N_2 atmosphere to obtain the final catalyst [Pd/Al_2O_3].

[Pd/Al_2O_3-x%] materials, where x% is the Pd loading (wt %), were obtained using the required amounts of K_2PdCl_4 and γ-Al_2O_3 in each case and following the general method described previously. [Pd/Al_2O_3-x°C/min], calcined at different heating ramps (10 and 30 °C/min), and [Pd/Al_2O_3-x°C], calcined at different final calcination temperatures (300 and 600 °C), were also obtained following the general procedure with the corresponding variations. For the corresponding materials with different supports, the general procedure was followed, changing the γ-Al_2O_3 to CaO, MgO, ZrO_2, TiO_2, SiO_2, or ZnO. Commercial CaO and MgO supports were calcined before their use at 500 °C under air flow, for 2 h at a heating ramp of 5 °C/min, and commercial ZrO_2 was calcined before its use at 250 °C under air flow, for 3 h at a heating ramp of 3 °C/min. For the corresponding [metal/Al_2O_3] materials other than palladium, K_2PdCl_4 was replaced by the corresponding amounts of $FeCl_3$, $CoCl_2$, $Ni(NO_3)_2{\cdot}6H_2O$, $Zn(acac)_2$, $AgNO_3$, $RuCl_3$, and K_2PtCl_4 and the general method was followed, except for the Ru catalyst, which was directly heated in a stream of N_2 (100 mL/min) with a heating ramp of 1 °C/min to 450 °C, held at that temperature under H_2 for 2 h, and then cooled down to room temperature under a N_2 atmosphere. The other Metal/Al_2O_3 catalysts were activated before reaction by heating the solid powder in a stream of N_2 (100 mL/min) with a heating ramp of 2 °C/min to 200 °C for [Ag/Al_2O_3], 450 °C for [Pt/Al_2O_3], and 600 °C for [Fe/Al_2O_3], [Co/Al_2O_3], [Ni/Al_2O_3], and [Zn/Al_2O_3], held at that temperature under H_2 for 2 h, and then cooled down to room temperature under a N_2 atmosphere to obtain the final catalysts. The bimetallic [Pd(5%)−Zn(5%)/Al_2O_3] catalyst was prepared by impregnation of γ-Al_2O_3 (0.797 g) with a solution of K_2PdCl_4 (0.153 g, 0.47 mmol) and $Zn(acac)_2{\cdot}xH_2O$ (23.7 wt % Zn) (0.211 g, 0.76 mmol) in a mixture of water:acetone (1:10, 110 mL) and the general procedure was followed. The bimetallic [Pd(5%)−Zn(2.5%)/Al_2O_3] and [Pd(5%)−Zn(10%)/Al_2O_3] catalysts were prepared analogously, adapting γ-Al_2O_3 and $Zn(acac)_2{\cdot}xH_2O$ amounts to the required weight percentage.

General Procedure for the Synthesis of Imidazolones via Dehydrogenative Cyclization between *N,N'*-Disub-

https://doi.org/10.1021/acscatal.2c01423
ACS Catal. 2022, 12, 6906−6922

stituted Ureas and 1,2-Diols. A 7 mL glass vial containing a stirring bar was sequentially charged with the corresponding *N,N′*-disubstituted urea (0.5 mmol), 1,2-diol (1 mmol, 2 equiv), [Pd/Al_2O_3] (2 or 5 mol % Pd), ZnO (5 or 10 mol %), if indicated, and *n*-Bu_2O (1.0 mL) as the solvent under an air atmosphere. Afterward, the reaction vial was capped with a septum and placed into an aluminum block, which was preheated at 150 °C. After the indicated time (16, 24, or 90 h), the reaction vial was cooled down to room temperature, diluted with ethanol, and centrifuged, and the supernatant was analyzed by GC. Then, the solvent was evaporated under a reduced pressure, and the crude of the reaction was purified by neutral-alumina or silica gel column chromatography (*n*-hexane/AcOEt) to yield the desired cyclic product.

■ ASSOCIATED CONTENT

Supporting Information

The Supporting Information is available free of charge at https://pubs.acs.org/doi/10.1021/acscatal.2c01423.

Experimental procedures, optimization of reaction conditions, kinetic and mechanistic studies, additional experiments, compound and material characterization data, and NMR spectra of isolatedcompounds (PDF)

■ AUTHOR INFORMATION

Corresponding Authors

Jose R. Cabrero-Antonino − *Instituto de Tecnología Química (UPV-CSIC), Universitat Politècnica de València-Consejo Superior de Investigaciones Científicas, 46022 València, Spain*; Email: jcabrero@itq.upv.es

Rosa Adam − *Instituto de Tecnología Química (UPV-CSIC), Universitat Politècnica de València-Consejo Superior de Investigaciones Científicas, 46022 València, Spain; Departament de Química Orgànica, Facultat de Farmàcia, Universitat de València, 46100 València, Spain;* orcid.org/0000-0001-9392-7187; Email: rosa.adam@uv.es

Authors

Juan Camilo Arango-Daza − *Instituto de Tecnología Química (UPV-CSIC), Universitat Politècnica de València-Consejo Superior de Investigaciones Científicas, 46022 València, Spain*

Carles Lluna-Galán − *Instituto de Tecnología Química (UPV-CSIC), Universitat Politècnica de València-Consejo Superior de Investigaciones Científicas, 46022 València, Spain*

Luis Izquierdo-Aranda − *Instituto de Tecnología Química (UPV-CSIC), Universitat Politècnica de València-Consejo Superior de Investigaciones Científicas, 46022 València, Spain*

Complete contact information is available at: https://pubs.acs.org/10.1021/acscatal.2c01423

Author Contributions

This paper was written through the contributions of all authors. All authors have given approval to the final version of the manuscript.

Notes

The authors declare no competing financial interest.

■ ACKNOWLEDGMENTS

This work was supported by the SEJI program funded by Generalitat Valenciana (Subvencions Excelencia Juniors Investigadors, grants SEJI/2019/006 and SEJI/2020/013), RETOS I+D+I program from MICINN (PID2019-109656RA-I0/AEI/10.13039/501100011033), and a program from "La Caixa" Foundation (ID 100010434), fellowship code LCF/BQ/PI18/11630023. J.R.C.-A. and R.A. are grateful to MICINN (Spanish Government) for two Ramón y Cajal contracts (ref RYC-2017-22717 and RYC2020-029493-I). The authors thank Dr. María Cabrero-Antonino for the fruitful discussions.

■ REFERENCES

(1) (a) Yamaguchi, R.; Fujita, K.-i.; Zhu, M. Recent Progress of New Catalytic Synthetic Methods for Nitrogen Heterocycles Based on Hydrogen Transfer Reactions. *Heterocycles* **2010**, *81*, 1093−1140. (b) Daştan, A.; Kulkarni, A.; Török, B. Environmentally Benign Synthesis of Heterocyclic Compounds by Combined Microwave-Assisted Heterogeneous Catalytic Approaches. *Green Chem.* **2012**, *14*, 17−37. (c) Nandakumar, A.; Midya, S. P.; Landge, V. G.; Balaraman, E. Transition-Metal-Catalyzed Hydrogen-Transfer Annulations: Access to Heterocyclic Scaffolds. *Angew. Chem., Int. Ed.* **2015**, *54*, 11022−11034. (d) Santhoshkumar, R.; Cheng, C.-H. Reaching Green: Heterocycle Synthesis by Transition Metal-Catalyzed C-H Functionalization in Sustainable Medium. *Chem. - Eur. J.* **2019**, *25*, 9366−9384. (e) Sreedevi, R.; Saranya, S.; Rohit, K. R.; Anilkumar, G. Recent Trends in Iron-Catalyzed Reactions Towards the Synthesis of Nitrogen-Containing Heterocycles. *Adv. Synth. Catal.* **2019**, *361*, 2236−2249. (f) Wang, S.; Xi, C. Recent Advances in Nucleophile-Triggered CO_2-Incorporated Cyclization Leading to Heterocycles. *Chem. Soc. Rev.* **2019**, *48*, 382−404. (g) Xiong, P.; Xu, H.-C. Chemistry with Electrochemically Generated N-Centered Radicals. *Acc. Chem. Res.* **2019**, *52*, 3339−3350. (h) Chen, Z.; Wang, L.-C.; Wu, X.-F. Carbonylative Synthesis of Heterocycles Involving Diverse Co Surrogates. *Chem. Commun.* **2020**, *56*, 6016−6030. (i) Vachan, B. S.; Karuppasamy, M.; Vinoth, P.; Vivek Kumar, S.; Perumal, S.; Sridharan, V.; Menendez, J. C. Proline and Its Derivatives as Organocatalysts for Multi-Component Reactions in Aqueous Media: Synergic Pathways to the Green Synthesis of Heterocycles. *Adv. Synth. Catal.* **2020**, *362*, 87−110. (j) Gulati, S.; John, S. E.; Shankaraiah, N. Microwave-Assisted Multicomponent Reactions in Heterocyclic Chemistry and Mechanistic Aspects. *Beilstein J. Org. Chem.* **2021**, *17*, 819−865. (k) Nishanth Rao, R.; Jena, S.; Mukherjee, M.; Maiti, B.; Chanda, K. Green Synthesis of Biologically Active Heterocycles of Medicinal Importance: A Review. *Environ. Chem. Lett.* **2021**, *19*, 3315−3358. (l) Singh, P. P.; Singh, P. K.; Beg, M. Z.; Kashyap, A.; Srivastava, V. Recent Applications of Photoredox Catalysis in O-Heterocycles: A Short Review. *Synth. Commun.* **2021**, *51*, 3033−3058. (m) Maji, M.; Panja, D.; Borthakur, I.; Kundu, S. Recent Advances in Sustainable Synthesis of N-Heterocycles Following Acceptorless Dehydrogenative Coupling Protocol Using Alcohols. *Org. Chem. Front.* **2021**, *8*, 2673−2709.

(2) (a) Dobereiner, G. E.; Crabtree, R. H. Dehydrogenation as a Substrate-Activating Strategy in Homogeneous Transition-Metal Catalysis. *Chem. Rev.* **2010**, *110*, 681−703. (b) Gunanathan, C.; Milstein, D. Applications of Acceptorless Dehydrogenation and Related Transformations in Chemical Synthesis. *Science* **2013**, *341*, No. 1229712. (c) Yang, Q.; Wang, Q.; Yu, Z. Substitution of Alcohols by N-Nucleophiles Via Transition Metal-Catalyzed Dehydrogenation. *Chem. Soc. Rev.* **2015**, *44*, 2305−2329. (d) Hakim Siddiki, S. M. A.; Toyao, T.; Shimizu, K.-i. Acceptorless Dehydrogenative Coupling Reactions with Alcohols over Heterogeneous Catalysts. *Green Chem.* **2018**, *20*, 2933−2952. (e) Paul, B.; Maji, M.; Chakrabarti, K.; Kundu, S. Tandem Transformations and Multicomponent Reactions Utilizing Alcohols Following Dehydrogenation Strategy. *Org. Biomol. Chem.* **2020**, *18*, 2193−2294. (f) Waiba, S.; Maji, B. Manganese Catalyzed Acceptorless Dehydrogenative Coupling Reactions. *ChemCatChem* **2020**, *12*, 1891−1902.

(3) (a) Tsuji, Y.; Huh, K. T.; Watanabe, Y. Ruthenium-Complex-Catalyzed N-Heterocyclization. Syntheses of Quinolines and Indole Derivatives from Aminoarenes and 1,3-Propanediol of Glycols. *J. Org.*

Chem. **1987**, *52*, 1673−1680. (b) Tsuji, Y.; Kotachi, S.; Huh, K. T.; Watanabe, Y. Ruthenium-Catalyzed Dehydrogenative N-Heterocyclization. Indoles from 2-Aminophenethyl Alcohols and 2-Nitrophenethyl Alcohols. *J. Org. Chem.* **1990**, *55*, 580−584. (c) Kondo, T.; Yang, S.; Huh, K. T.; Kobayashi, M.; Kotachi, S.; Watanabe, Y. Ruthenium Complex-Catalyzed Facile Synthesis of 2-Substituted Benzoazoles. *Chem. Lett.* **1991**, *20*, No. 1275. (d) Kondo, T.; Kotachi, S.; Watanabe, Y. Ruthenium Complex-Catalysed Synthesis of 1,3-Disubstituted 2,3-Dihydroimidazol-2-ones from *N,N′*-Disubstituted Ureas and Vicinal Diols. *J. Chem. Soc., Chem. Commun.* **1992**, 1318−1319. (e) Tursky, M.; Lorentz-Petersen, L. L. R.; Olsen, L. B.; Madsen, R. Iridium- and Ruthenium-Catalysed Synthesis of 2,3-Disubstituted Indoles from Anilines and Vicinal Diols. *Org. Biomol. Chem.* **2010**, *8*, 5576−5582. (f) Gnanaprakasam, B.; Balaraman, E.; Ben-David, Y.; Milstein, D. Synthesis of Peptides and Pyrazines from *β*-Amino Alcohols through Extrusion of H_2 Catalyzed by Ruthenium Pincer Complexes: Ligand-Controlled Selectivity. *Angew. Chem., Int. Ed.* **2011**, *50*, 12240−12244. (g) Iida, K.; Miura, T.; Ando, J.; Saito, S. The Dual Role of Ruthenium and Alkali Base Catalysts in Enabling a Conceptually New Shortcut to N-Unsubstituted Pyrroles through Unmasked *α*-Amino Aldehydes. *Org. Lett.* **2013**, *15*, 1436−1439. (h) Srimani, D.; Ben-David, Y.; Milstein, D. Direct Synthesis of Pyrroles by Dehydrogenative Coupling of *β*-Aminoalcohols with Secondary Alcohols Catalyzed by Ruthenium Pincer Complexes. *Angew. Chem., Int. Ed.* **2013**, *52*, 4012−4015. (i) Zhang, M.; Fang, X.; Neumann, H.; Beller, M. General and Regioselective Synthesis of Pyrroles Via Ruthenium-Catalyzed Multicomponent Reactions. *J. Am. Chem. Soc.* **2013**, *135*, 11384−11388.

(4) (a) Whitney, S.; Grigg, R.; Derrick, A.; Keep, A. $[Cp^*IrCl_2]_2$-Catalyzed Indirect Functionalization of Alcohols: Novel Strategies for the Synthesis of Substituted Indoles. *Org. Lett.* **2007**, *9*, 3299−3302. (b) Aramoto, H.; Obora, Y.; Ishii, Y. N-Heterocyclization of Naphthylamines with 1,2- and 1,3-Diols Catalyzed by an Iridium Chloride/BINAP System. *J. Org. Chem.* **2009**, *74*, 628−633. (c) Zhou, J.; Fang, J. One-Pot Synthesis of Quinazolinones Via Iridium-Catalyzed Hydrogen Transfers. *J. Org. Chem.* **2011**, *76*, 7730−7736. (d) Michlik, S.; Kempe, R. A Sustainable Catalytic Pyrrole Synthesis. *Nat. Chem.* **2013**, *5*, 140−144.

(5) (a) Daw, P.; Chakraborty, S.; Garg, J. A.; Ben-David, Y.; Milstein, D. Direct Synthesis of Pyrroles by Dehydrogenative Coupling of Diols and Amines Catalyzed by Cobalt Pincer Complexes. *Angew. Chem., Int. Ed.* **2016**, *55*, 14373−14377. (b) Midya, S. P.; Landge, V. G.; Sahoo, M. K.; Rana, J.; Balaraman, E. Cobalt-Catalyzed Acceptorless Dehydrogenative Coupling of Aminoalcohols with Alcohols: Direct Access to Pyrrole, Pyridine and Pyrazine Derivatives. *Chem. Commun.* **2018**, *54*, 90−93. (c) Shee, S.; Ganguli, K.; Jana, K.; Kundu, S. Cobalt Complex Catalyzed Atom-Economical Synthesis of Quinoxaline, Quinoline and 2-Alkylaminoquinoline Derivatives. *Chem. Commun.* **2018**, *54*, 6883−6886.

(6) (a) Kallmeier, F.; Dudziec, B.; Irrgang, T.; Kempe, R. Manganese-Catalyzed Sustainable Synthesis of Pyrroles from Alcohols and Amino Alcohols. *Angew. Chem., Int. Ed.* **2017**, *56*, 7261−7265. (b) Mastalir, M.; Glatz, M.; Pittenauer, E.; Allmaier, G.; Kirchner, K. Sustainable Synthesis of Quinolines and Pyrimidines Catalyzed by Manganese PNP Pincer Complexes. *J. Am. Chem. Soc.* **2016**, *138*, 15543−15546.

(7) For remarkable examples affording pyrimidines, quinolines and indoles using heterogeneous catalysis see: (a) He, L.; Wang, J.-Q.; Gong, Y.; Liu, Y.-M.; Cao, Y.; He, H.-Y.; Fan, K.-N. Titania-Supported Iridium Subnanoclusters as an Efficient Heterogeneous Catalyst for Direct Synthesis of Quinolines from Nitroarenes and Aliphatic Alcohols. *Angew. Chem., Int. Ed.* **2011**, *50*, 10216−10220. (b) Shimura, S.; Miura, H.; Wada, K.; Hosokawa, S.; Yamazoe, S.; Inoue, M. Ceria-Supported Ruthenium Catalysts for the Synthesis of Indole Via Dehydrogenative N-Heterocyclization. *Catal. Sci. Technol.* **2011**, *1*, 1340−1346. (c) Llabres-Campaner, P. J.; Ballesteros-Garrido, R.; Ballesteros, R.; Abarca, B. Straight Access to Indoles from Anilines and Ethylene Glycol by Heterogeneous Acceptorless Dehydrogenative Condensation. *J. Org. Chem.* **2018**, *83*, 521−526. (d) Sultana Poly, S.; Siddiki, S. M. A. H.; Touchy, A. S.; Ting, K. W.; Toyao, T.; Maeno, Z.; Kanda, Y.; Shimizu, K.-i. Acceptorless Dehydrogenative Synthesis of Pyrimidines from Alcohols and Amidines Catalyzed by Supported Platinum Nanoparticles. *ACS Catal.* **2018**, *8*, 11330−11341. (e) Chaurasia, S. R.; Tiwari, A. R.; Bhanage, B. M. Synthesis of Quinolines Via Acceptorless Dehydrogenative Tandem Cyclization of 2-Aminobenzyl Alcohol with Alcohols Using Magnetic CuNiFeO Nanocatalyst. *Mol. Catal.* **2019**, *478*, No. 110565. (f) Chaudhari, C.; Sato, K.; Ogura, Y.; Miayahara, S.-I.; Nagaoka, K. Pr_2O_3 Supported Nano-Layered Ruthenium Catalyzed Acceptorless Dehydrogenative Synthesis of 2-Substituted Quinolines and 1,8-Naphthyridines from 2-Aminoaryl Alcohols and Ketones. *ChemCatChem* **2020**, *12*, 2198−2202. (g) Bellezza, D.; Zaragozá, R. J.; José Aurell, M.; Ballesteros, R.; Ballesteros-Garrido, R. Acceptorless Dehydrogenative Condensation: Synthesis of Indoles and Quinolines from Diols and Anilines. *Org. Biomol. Chem.* **2021**, *19*, 677−683.

(8) Schnettler, R. A.; Dage, R. C.; Grisar, J. M. 4-Aryl-1,3-dihydro-2H-imidazol-2-ones, a New Class of Cardiotonic Agents. *J. Med. Chem.* **1982**, *25*, 1477−1481.

(9) Vardanyan, R.; Hruby, V. Antipsychotics. In *Synthesis of Best-Seller Drugs*, Vardanyan, R.; Hruby, V., Eds.; Academic Press: Boston, 2016; Chapter 6, pp 87−110.

(10) (a) Juruena, M. F.; Pondé de Sena, E.; Reis De Oliveira, I. Sertindole in the Management of Schizophrenia. *J. Cent. Nerv. Syst. Dis.* **2011**, *3*, 75−85. (b) Smyj, R.; Wang, X.-P.; Han, F. Pimozide. In *Profiles of Drug Substances, Excipients and Related Methodology*, Brittain, H. G., Ed.; Academic Press, 2012; Chapter 7, Vol. 37, pp 287−311.

(11) Chang, C.-S.; Lin, Y.-T.; Shih, S.-R.; Lee, C.-C.; Lee, Y.-C.; Tai, C.-L.; Tseng, S.-N.; Chern, J.-H. Design, Synthesis, and Antipicornavirus Activity of 1-[5-(4-Arylphenoxy)alkyl]-3-Pyridin-4-Ylimidazolidin-2-one Derivatives. *J. Med. Chem.* **2005**, *48*, 3522−3535.

(12) Bronson, J. J.; DenBleyker, K. L.; Falk, P. J.; Mate, R. A.; Ho, H.-T.; Pucci, M. J.; Snyder, L. B. Discovery of the First Antibacterial Small Molecule Inhibitors of Murb. *Bioorg. Med. Chem. Lett.* **2003**, *13*, 873−875.

(13) Pettit, G. R.; McNulty, J.; Herald, D. L.; Doubek, D. L.; Chapuis, J.-C.; Schmidt, J. M.; Tackett, L. P.; Boyd, M. R. Antineoplastic Agents. 362. Isolation and X-Ray Crystal Structure of Dibromophakellstatin from the Indian Ocean Sponge Phakellia Mauritiana. *J. Nat. Prod.* **1997**, *60*, 180−183.

(14) De Clercq, P. J. Biotin: A Timeless Challenge for Total Synthesis. *Chem. Rev.* **1997**, *97*, 1755−1792.

(15) (a) Verniest, G.; Padwa, A. Gold- and Silver-Mediated Cycloisomerizations of N-Propargylamides. *Org. Lett.* **2008**, *10*, 4379−4382. (b) Peshkov, V. A.; Pereshivko, O. P.; Sharma, S.; Meganathan, T.; Parmar, V. S.; Ermolat'ev, D. S.; Van der Eycken, E. V. Tetrasubstituted 2-Imidazolones Via Ag(I)-Catalyzed Cycloisomerization of Propargylic Ureas. *J. Org. Chem.* **2011**, *76*, 5867−5872. (c) Pereshivko, O. P.; Peshkov, V. A.; Jacobs, J.; Meervelt, L. V.; Van der Eycken, E. V. Cationic Gold- and Silver-Catalyzed Cycloisomerizations of Propargylic Ureas: A Selective Entry to Oxazolidin-2-imines and Imidazolidin-2-ones. *Adv. Synth. Catal.* **2013**, *355*, 781−789. (d) Arrowsmith, M.; Hill, M. S.; Kociok-Köhn, G. Group 2 Catalysis for the Atom-Efficient Synthesis of Imidazolidine and Thiazolidine Derivatives. *Chem. - Eur. J.* **2015**, *21*, 10548−10557. (e) La-Venia, A.; Medran, N. S.; Krchňák, V.; Testero, S. A. Synthesis of a Small Library of Imidazolidin-2-ones Using Gold Catalysis on Solid Phase. *ACS Comb. Sci.* **2016**, *18*, 482−489. (f) Casnati, A.; Perrone, A.; Mazzeo, P. P.; Bacchi, A.; Mancuso, R.; Gabriele, B.; Maggi, R.; Maestri, G.; Motti, E.; Stirling, A.; Ca', N. D. Synthesis of Imidazolidin-2-ones and Imidazol-2-ones Via Base-Catalyzed Intramolecular Hydroamidation of Propargylic Ureas under Ambient Conditions. *J. Org. Chem.* **2019**, *84*, 3477−3490. (g) Zuliani, A.; Ranjan, P.; Luque, R.; Van der Eycken, E. V. Heterogeneously Catalyzed Synthesis of Imidazolones Via Cycloisomerizations of Propargylic Ureas Using Ag and Au/Al SBA-15 Systems. *ACS Sustainable Chem. Eng.* **2019**, *7*, 5568−5575.

https://doi.org/10.1021/acscatal.2c01423
ACS Catal. 2022, 12, 6906−6922

(16) (a) Zhao, B.; Du, H.; Shi, Y. Cu(I)-Catalyzed C−H α-Amination of Aryl Ketones: Direct Synthesis of Imidazolinones. *J. Org. Chem.* **2009**, *74*, 4411−4413. (b) Zhu, Y.; Shi, Y. CuI-Catalyzed Sequential Diamination and Dehydrogenation of Terminal Olefins: A Facile Approach to Imidazolinones. *Chem. - Eur. J.* **2014**, *20*, 13901−13904.
(17) (a) Gabriele, B.; Salerno, G.; Mancuso, R.; Costa, M. Efficient Synthesis of Ureas by Direct Palladium-Catalyzed Oxidative Carbonylation of Amines. *J. Org. Chem.* **2004**, *69*, 4741−4750. (b) Kimura, T.; Kamata, K.; Mizuno, N. A Bifunctional Tungstate Catalyst for Chemical Fixation of CO_2 at Atmospheric Pressure. *Angew. Chem., Int. Ed.* **2012**, *51*, 6700−6703. (c) Yu, B.; Zhang, H.; Zhao, Y.; Chen, S.; Xu, J.; Hao, L.; Liu, Z. DBU-based Ionic-Liquid-Catalyzed Carbonylation of O-Phenylenediamines with CO_2 to 2-Benzimidazolones under Solvent-Free Conditions. *ACS Catal.* **2013**, *3*, 2076−2082.
(18) Shi, M.; Shen, Y.-M. Transition-Metal-Catalyzed Reactions of Propargylamine with Carbon Dioxide and Carbon Disulfide. *J. Org. Chem.* **2002**, *67*, 16−21.
(19) Chuprakov, S.; Kwok, S. W.; Fokin, V. V. Transannulation of 1-Sulfonyl-1,2,3-Triazoles with Heterocumulenes. *J. Am. Chem. Soc.* **2013**, *135*, 4652−4655.
(20) Kise, N.; Goi, S.; Sakurai, T. Reductive Coupling of Hydantoins with Benzophenones by Low-Valent Titanium: Synthesis of 4-Substituted 1*H*-Imidazol-2(3*H*)-ones and Unusual Two-to-Two Coupled Products. *Tetrahedron* **2018**, *74*, 992−1001.
(21) Peña-López, M.; Neumann, H.; Beller, M. (Enantio)Selective Hydrogen Autotransfer: Ruthenium-Catalyzed Synthesis of Oxazolidin-2-ones from Urea and Diols. *Angew. Chem., Int. Ed.* **2016**, *55*, 7826−7830.
(22) (a) Abarca, B.; Adam, R.; Ballesteros, R. An Efficient One Pot Transfer Hydrogenation and N-Alkylation of Quinolines with Alcohols Mediated by Pd/C/Zn. *Org. Biomol. Chem.* **2012**, *10*, 1826−1833. (b) Bou-Puerto, A.; Bellezza, D.; Martinez-Morro, C.; Gonzalez-Sanchis, N.; Ballesteros, R.; Cuñat, A. C.; Ballesteros-Garrido, R. 6-Amino-7-Azaindoles Synthesis from 2,6-Diamino Pyridine and Diols. *Tetrahedron Lett.* **2021**, *84*, No. 153460.
(23) Guo, B.; Li, H.-X.; Zhang, S.-Q.; Young, D. J.; Lang, J.-P. C-N Bond Formation Catalyzed by Ruthenium Nanoparticles Supported on N-Doped Carbon Via Acceptorless Dehydrogenation to Secondary Amines, Imines, Benzimidazoles and Quinoxalines. *ChemCatChem* **2018**, *10*, 5627−5636.
(24) (a) He, J.; Kim, J. W.; Yamaguchi, K.; Mizuno, N. Efficient Catalytic Synthesis of Tertiary and Secondary Amines from Alcohols and Urea. *Angew. Chem., Int. Ed.* **2009**, *48*, 9888−9891. (b) Yamaguchi, K.; He, J.; Oishi, T.; Mizuno, N. The "Borrowing Hydrogen Strategy" by Supported Ruthenium Hydroxide Catalysts: Synthetic Scope of Symmetrically and Unsymmetrically Substituted Amines. *Chem. - Eur. J.* **2010**, *16*, 7199−7207.
(25) For selected examples of Ag, Pd, Pt, Ni or V nanoparticles over Al_2O_3 support active in dehydrogenative processes see: (a) Shimizu, K.-i.; Ohshima, K.; Satsuma, A. Direct Dehydrogenative Amide Synthesis from Alcohols and Amines Catalyzed by γ-Alumina Supported Silver Cluster. *Chem. - Eur. J.* **2009**, *15*, 9977−9980. (b) Shimizu, K.-i.; Sato, R.; Satsuma, A. Direct C-C Cross-Coupling of Secondary and Primary Alcohols Catalyzed by a γ-Alumina-Supported Silver Subnanocluster. *Angew. Chem., Int. Ed.* **2009**, *48*, 3982−3986. (c) Shimizu, K.-i.; Shimura, K.; Ohshima, K.; Tamura, M.; Satsuma, A. Selective Cross-Coupling of Amines by Alumina-Supported Palladium Nanocluster Catalysts. *Green Chem.* **2011**, *13*, 3096−3100. (d) Kon, K.; Hakim Siddiki, S. M. A.; Shimizu, K.-i. Size- and Support-Dependent Pt Nanocluster Catalysis for Oxidant-Free Dehydrogenation of Alcohols. *J. Catal.* **2013**, *304*, 63−71. (e) Shimizu, K.-i.; Imaiida, N.; Kon, K.; Hakim Siddiki, S. M. A.; Satsuma, A. Heterogeneous Ni Catalysts for N-Alkylation of Amines with Alcohols. *ACS Catal.* **2013**, *3*, 998−1005. (f) Shimizu, K.-i.; Kon, K.; Onodera, W.; Yamazaki, H.; Kondo, J. N. Heterogeneous Ni Catalyst for Direct Synthesis of Primary Amines from Alcohols and Ammonia. *ACS Catal.* **2013**, *3*, 112−117. (g) Shimizu, K.-i.; Kon, K.; Shimura, K.; Hakim, S. S. M. A. Acceptor-Free Dehydrogenation of Secondary Alcohols by Heterogeneous Cooperative Catalysis between Ni Nanoparticles and Acid−Base Sites of Alumina Supports. *J. Catal.* **2013**, *300*, 242−250. (h) Siddiki, S. M. A. H.; Kon, K.; Shimizu, K.-i. General and Selective C-3 Alkylation of Indoles with Primary Alcohols by a Reusable Pt Nanocluster Catalyst. *Chem. - Eur. J.* **2013**, *19*, 14416−14419. (i) Kon, K.; Onodera, W.; Toyao, T.; Shimizu, K.-i. Supported Rhenium Nanoparticle Catalysts for Acceptorless Dehydrogenation of Alcohols: Structure−Activity Relationship and Mechanistic Studies. *Catal. Sci. Technol.* **2016**, *6*, 5864−5870. (j) Zhao, Z.-J.; Wu, T.; Xiong, C.; Sun, G.; Mu, R.; Zeng, L.; Gong, J. Hydroxyl-Mediated Non-Oxidative Propane Dehydrogenation over VO_x/γ-Al_2O_3 Catalysts with Improved Stability. *Angew. Chem., Int. Ed.* **2018**, *57*, 6791−6795.
(26) Shimizu, K.-i.; Sugino, K.; Sawabe, K.; Satsuma, A. Oxidant-Free Dehydrogenation of Alcohols Heterogeneously Catalyzed by Cooperation of Silver Clusters and Acid−Base Sites on Alumina. *Chem. - Eur. J.* **2009**, *15*, 2341−2351.
(27) Shimura, K.; Shimizu, K.-i. Transfer Hydrogenation of Ketones by Ceria-Supported Ni Catalysts. *Green Chem.* **2012**, *14*, 2983−2985.
(28) (a) Bhogeswararao, S.; Srinivas, D. Catalytic Conversion of Furfural to Industrial Chemicals over Supported Pt and Pd Catalysts. *J. Catal.* **2015**, *327*, 65−77. (b) Kim, K. D.; Wang, Z.; Tao, Y.; Ling, H.; Yuan, Y.; Zhou, C.; Liu, Z.; Gaborieau, M.; Huang, J.; Yu, A. The Comparative Effect of Particle Size and Support Acidity on Hydrogenation of Aromatic Ketones. *ChemCatChem* **2019**, *11*, 4810−4817.
(29) Holder, C. F.; Schaak, R. E. Tutorial on Powder X-Ray Diffraction for Characterizing Nanoscale Materials. *ACS Nano* **2019**, *13*, 7359−7365.
(30) (a) Otto, K.; Hubbard, C. P.; Weber, W. H.; Graham, G. W. Raman Spectroscopy of Palladium Oxide on γ-Alumina Applicable to Automotive Catalysts: Nondestructive, Quantitative Analysis; Oxidation Kinetics; Fluorescence Quenching. *Appl. Catal., B* **1992**, *1*, 317−327. (b) Baylet, A.; Marécot, P.; Duprez, D.; Castellazzi, P.; Groppi, G.; Forzatti, P. In Situ Raman and In Situ XRD Analysis of PdO Reduction and Pd° Oxidation Supported on γ-Al_2O_3 Catalyst under Different Atmospheres. *Phys. Chem. Chem. Phys.* **2011**, *13*, 4607−4613.
(31) García-Zaleta, D. S.; Torres-Huerta, A. M.; Domínguez-Crespo, M. A.; García-Murillo, A.; Silva-Rodrigo, R.; González, R. L. Influence of Phases Content on Pt/TiO_2, Pd/TiO_2 Catalysts for Degradation of 4-Chlorophenol at Room Temperature. *J. Nanomater.* **2016**, *2016*, No. 1805169.
(32) Akuri, S. R.; Dhoke, C.; Rakesh, K.; Hegde, S.; Nair, S. A.; Deshpande, R.; Manikandan, P. Decomposition of Methyl Formate over Supported Pd Catalysts. *Catal. Lett.* **2017**, *147*, 1285−1293.
(33) Claus, P.; Berndt, H.; Mohr, C.; Radnik, J.; Shin, E.-J.; Keane, M. A. Pd/MgO: Catalyst Characterization and Phenol Hydrogenation Activity. *J. Catal.* **2000**, *192*, 88−97.
(34) Ivanova, A. S.; Slavinskaya, E. M.; Gulyaev, R. V.; Zaikovskii, V. I.; Stonkus, O. A.; Danilova, I. G.; Plyasova, L. M.; Polukhina, I. A.; Boronin, A. I. Metal−Support Interactions in Pt/Al_2O_3 and Pd/Al_2O_3 Catalysts for CO Oxidation. *Appl. Catal., B* **2010**, *97*, 57−71.
(35) Llabres-Campaner, P. J.; Woodbridge-Ortega, P.; Ballesteros-Garrido, R.; Ballesteros, R.; Abarca, B. Heterogeneous Borrowing Hydrogen Reactions with Pd/C and ZnO: Diol Scope. *Tetrahedron Lett.* **2017**, *58*, 4880−4882.
(36) (a) Bahruji, H.; Bowker, M.; Hutchings, G.; Dimitratos, N.; Wells, P.; Gibson, E.; Jones, W.; Brookes, C.; Morgan, D.; Lalev, G. Pd/ZnO Catalysts for Direct CO_2 Hydrogenation to Methanol. *J. Catal.* **2016**, *343*, 133−146. (b) Bahruji, H.; Esquius, J. R.; Bowker, M.; Hutchings, G.; Armstrong, R. D.; Jones, W. Solvent Free Synthesis of $PdZn/TiO_2$ Catalysts for the Hydrogenation of CO_2 to Methanol. *Top. Catal.* **2018**, *61*, 144−153.
(37) (a) Iwasa, N.; Masuda, S.; Ogawa, N.; Takezawa, N. Steam Reforming of Methanol over Pd/ZnO: Effect of the Formation of PdZn Alloys Upon the Reaction. *Appl. Catal., A* **1995**, *125*, 145−157. (b) Iwasa, N.; Takezawa, N. New Supported Pd and Pt Alloy Catalysts for Steam Reforming and Dehydrogenation of Methanol.

https://doi.org/10.1021/acscatal.2c01423
ACS Catal. 2022, 12, 6906−6922

Top. Catal. **2003**, *22*, 215−224. (c) Karim, A.; Conant, T.; Datye, A. The Role of PdZn Alloy Formation and Particle Size on the Selectivity for Steam Reforming of Methanol. *J. Catal.* **2006**, *243*, 420−427. (d) Zhang, Q.; Farrauto, R. J. A PdZn Catalyst Supported on Stabilized Ceria for Stoichiometric Methanol Steam Reforming and Hydrogen Production. *Appl. Catal., A* **2011**, *395*, 64−70.

(38) (a) González-Fernández, A.; Berenguer-Murcia, Á.; Cazorla-Amorós, D.; Cárdenas-Lizana, F. Zn-Promoted Selective Gas-Phase Hydrogenation of Tertiary and Secondary C4 Alkynols over Supported Pd. *ACS Appl. Mater. Interfaces* **2020**, *12*, 28158−28168. (b) Tew, M. W.; Emerich, H.; van Bokhoven, J. A. Formation and Characterization of PdZn Alloy: A Very Selective Catalyst for Alkyne Semihydrogenation. *J. Phys. Chem. C* **2011**, *115*, 8457−8465.

(39) Williams, W. L.; Zeng, L.; Gensch, T.; Sigman, M. S.; Doyle, A. G.; Anslyn, E. V. The Evolution of Data-Driven Modeling in Organic Chemistry. *ACS Cent. Sci.* **2021**, *7*, 1622−1637.

(40) (a) Cotter, L. F.; Brown, P. J.; Nelson, R. C.; Takematsu, K. Divergent Hammett Plots of the Ground- and Excited-State Proton Transfer Reactions of 7-Substituted-2-Naphthol Compounds. *J. Phys. Chem. B* **2019**, *123*, 4301−4310. (b) Davis-Gilbert, Z. W.; Wen, X.; Goodpaster, J. D.; Tonks, I. A. Mechanism of Ti-Catalyzed Oxidative Nitrene Transfer in [2 + 2 + 1] Pyrrole Synthesis from Alkynes and Azobenzene. *J. Am. Chem. Soc.* **2018**, *140*, 7267−7281. (c) Schreck, J. O. Nonlinear Hammett Relationships. *J. Chem. Educ.* **1971**, *48*, 103.

https://doi.org/10.1021/acscatal.2c01423
ACS Catal. 2022, 12, 6906−6922